









TECH BRIEFS

NATIONAL AERONAUTICS AND SPACE ADMINISTRATION

-  **Technology Focus**
-  **Electronics/Computers**
-  **Software**
-  **Materials**
-  **Mechanics**
-  **Machinery/Automation**
-  **Manufacturing**
-  **Bio-Medical**
-  **Physical Sciences**
-  **Information Sciences**
-  **Books and Reports**

INTRODUCTION

Tech Briefs are short announcements of innovations originating from research and development activities of the National Aeronautics and Space Administration. They emphasize information considered likely to be transferable across industrial, regional, or disciplinary lines and are issued to encourage commercial application.

Availability of NASA Tech Briefs and TSPs

Requests for individual Tech Briefs or for Technical Support Packages (TSPs) announced herein should be addressed to

National Technology Transfer Center

Telephone No. (800) 678-6882 or via World Wide Web at www2.nttc.edu/leads/

Please reference the control numbers appearing at the end of each Tech Brief. Information on NASA's Commercial Technology Team, its documents, and services is also available at the same facility or on the World Wide Web at www.nctn.hq.nasa.gov.

Commercial Technology Offices and Patent Counsels are located at NASA field centers to provide technology-transfer access to industrial users. Inquiries can be made by contacting NASA field centers and program offices listed below.

NASA Field Centers and Program Offices

Ames Research Center

Carolina Blake
(650) 604-1754
carolina.m.blake@nasa.gov

Dryden Flight Research Center

Jenny Baer-Riedhart
(661) 276-3689
jenny.baer-riedhart@dfrc.nasa.gov

Goddard Space Flight Center

Nona Cheeks
(301) 286-5810
Nona.K.Cheeks.1@gssc.nasa.gov

Jet Propulsion Laboratory

Art Murphy, Jr.
(818) 354-3480
arthur.j.murphy-jr@jpl.nasa.gov

Johnson Space Center

Charlene E. Gilbert
(281) 483-3809
commercialization@jsc.nasa.gov

Kennedy Space Center

Jim Aliberti
(321) 867-6224
Jim.Aliberti-1@ksc.nasa.gov

Langley Research Center

Jesse Midgett
(757) 864-3936
jesse.c.midgett@nasa.gov

John H. Glenn Research Center at Lewis Field

Larry Viterna
(216) 433-3484
cto@grc.nasa.gov

Marshall Space Flight Center

Vernotto McMillan
(256) 544-2615
vernotto.mcmillan@msfc.nasa.gov

Stennis Space Center

Robert Bruce
(228) 688-1929
robert.c.bruce@nasa.gov

NASA Program Offices

At NASA Headquarters there are seven major program offices that develop and oversee technology projects of potential interest to industry:

Carl Ray

Small Business Innovation Research Program (SBIR) & Small Business Technology Transfer Program (STTR)
(202) 358-4652 or
cray@mail.hq.nasa.gov

Benjamin Neumann

Innovative Technology Transfer Partnerships (Code RP)
(202) 358-2320
benjamin.j.neumann@nasa.gov

John Mankins

Office of Space Flight (Code MP)
(202) 358-4659 or
jmankins@mail.hq.nasa.gov

Terry Hertz

Office of Aero-Space Technology (Code RS)
(202) 358-4636 or
thertz@mail.hq.nasa.gov

Glen Mucklow

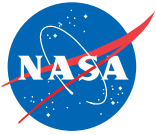
Office of Space Sciences (Code SM)
(202) 358-2235 or
gmucklow@mail.hq.nasa.gov

Roger Crouch

Office of Microgravity Science Applications (Code U)
(202) 358-0689 or
rcrouch@hq.nasa.gov

Granville Paules

Office of Mission to Planet Earth (Code Y)
(202) 358-0706 or
gpaules@mtpe.hq.nasa.gov



TECH BRIEFS

NATIONAL AERONAUTICS AND SPACE ADMINISTRATION



5 Technology Focus: Composites/Plastics

- 5 Embedded Heaters for Joining or Separating Plastic Parts
- 5 Curing Composite Materials Using Lower-Energy Electron Beams
- 6 Aluminum-Alloy-Matrix/Alumina-Reinforcement Composites
- 6 Fibrous-Ceramic/Aerogel Composite Insulating Tiles
- 7 Urethane/Silicone Adhesives for Bonding Flexing Metal Parts



9 Electronics/Computers

- 9 Scalable Architecture for Multihop Wireless ad Hoc Networks
- 10 Improved Thermoplastic/Iron-Particle Transformer Cores
- 11 Cooperative Lander-Surface/Aerial Microflyer Missions for Mars Exploration
- 12 Dual-Frequency Airborne Scanning Rain Radar Antenna System
- 13 Eight-Channel Continuous Timer
- 13 Reduction of Phase Ambiguity in an Offset-QPSK Receiver
- 14 Ambient-Light-Canceling Camera Using Subtraction of Frames
- 15 Lightweight, Flexible, Thin, Integrated Solar-Power Packs



17 Software

- 17 Windows®-Based Software Models Cyclic Oxidation Behavior
- 17 Software for Analyzing Sequences of Flow-Related Images



19 Mechanics

- 19 Improved Ball-and-Socket Docking Mechanism
- 20 Two-Stage Solenoid



21 Manufacturing

- 21 Ordered Nanostructures Made Using Chaperonin Polypeptides
- 22 Low-Temperature Plasma Functionalization of Carbon Nanotubes



23 Physical Sciences

- 23 Improved Cryostat for Cooling a Wide Panel
- 23 Current Pulses Momentarily Enhance Thermoelectric Cooling
- 24 Hand-Held Color Meters Based on Interference Filters
- 25 Calculating Mass Diffusion in High-Pressure Binary Fluids
- 26 Fresnel Lenses for Wide-Aperture Optical Receivers



29 Information Sciences

- 29 Increasing Accuracy in Computed Inviscid Boundary Conditions
- 29 Higher-Order Finite Elements for Computing Thermal Radiation



31 Books & Reports

- 31 Radar for Monitoring Hurricanes From Geostationary Orbit
- 31 Time-Transfer System for Two Orbiting Spacecraft

This document was prepared under the sponsorship of the National Aeronautics and Space Administration. Neither the United States Government nor any person acting on behalf of the United States Government assumes any liability resulting from the use of the information contained in this document, or warrants that such use will be free from privately owned rights.



Embedded Heaters for Joining or Separating Plastic Parts

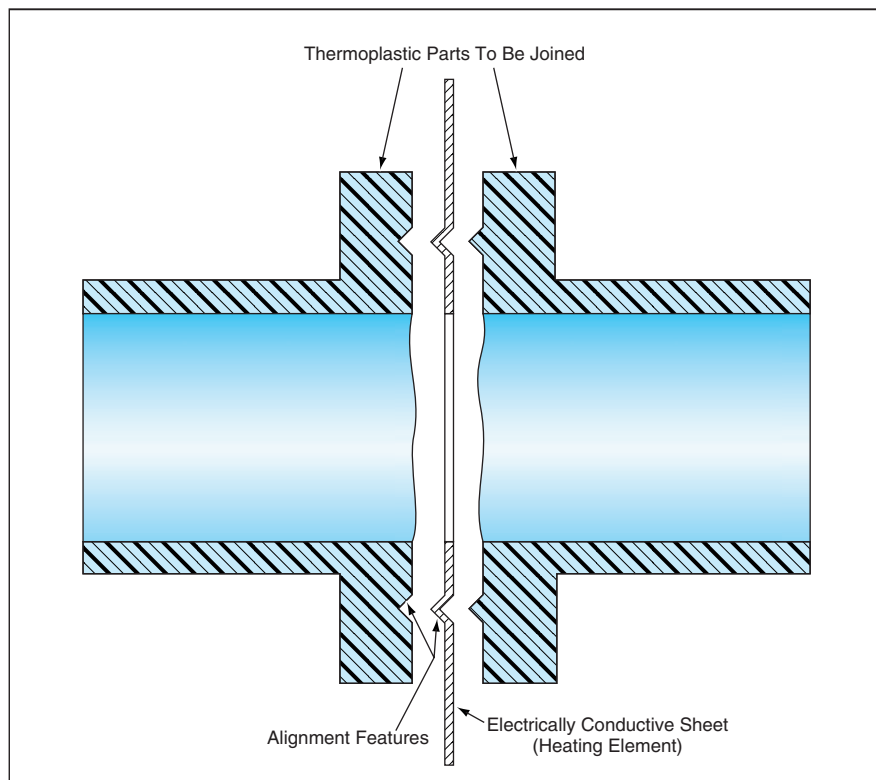
Bonding heat would be generated and applied locally.

Marshall Space Flight Center, Alabama

A proposed thermal-bonding technique would make it possible to join or separate thermoplastic parts quickly and efficiently. The technique would eliminate the need for conventional welding or for such conventional fastening components as bolted flanges or interlocking hooks. The technique could be particularly useful in the sign industry (in which large quantities of thermoplastics are used) or could be used to join plastic pipes.

A thin sheet of a suitable electrically conductive material would be formed to fit between two thermoplastic parts to be joined (see figure). The electrically conductive sheet and the two parts would be put together tightly, then an electrical current would be sent through the conductor to heat the thermoplastic locally. The magnitude of the current and the heating time would be chosen to generate just enough heat to cause the thermoplastic to adhere to both sides of the electrically conductive sheet. Optionally, the electrically conductive sheet could contain many small holes to provide purchase or to increase electrical resistance to facilitate the generation of heat.

After thermal bonding, the electrically conductive sheet remains as an integral part of the structure. If necessary, the electrically conductive sheet can be reheated later to separate the joined thermoplastic parts.



An Electrically Conductive Sheet would serve as a heating element to join two thermoplastic parts.

This work was done by Melvin A. Bryant III of Marshall Space Flight Center.

This invention has been patented by NASA (U.S. Patent No. 6,394,501). Inquiries concerning nonexclusive or exclusive license for its

commercial development should be addressed to Benita Hayes, MSFC Commercialization Assistance Lead, at benita.c.hayes@nasa.gov. Refer to MFS-31403.

Curing Composite Materials Using Lower-Energy Electron Beams

Less shielding is needed at lower beam energies.

Marshall Space Flight Center, Alabama

In an improved method of fabricating composite-material structures by laying up prepreg tapes (tapes of fiber reinforcement impregnated by uncured matrix materials) and then curing them, one cures the layups by use of beams of electrons having kinetic energies in the range of 200 to 300 keV. In contrast, in a prior

method, one used electron beams characterized by kinetic energies up to 20 MeV. The improved method was first suggested by an Italian group in 1993, but had not been demonstrated until recently.

With respect to both the prior method and the present improved method, the impetus for the use of elec-

tron-beam curing is a desire to avoid the high costs of autoclaves large enough to effect thermal curing of large composite-material structures. Unfortunately, in the prior method, the advantages of electron-beam curing are offset by the need for special walls and ceilings on curing chambers to shield personnel

from x rays generated by impacts of energetic electrons. These shields must be thick [typically 2 to 3 ft (about 0.6 to 0.9 m) if made of concrete] and are therefore expensive. They also make it difficult to bring large structures into and out of the curing chambers.

Currently, all major companies that fabricate composite-material spacecraft and aircraft structures form their layups by use of automated tape placement (ATP) machines. In the present improved method, an electron-beam gun is attached to an ATP head and used to irradiate the tape as it is pressed onto the workpiece. The elec-

tron kinetic energy between 200 and 300 keV is sufficient for penetration of the ply being laid plus one or two of the plies underneath it. Provided that the electron-beam gun is properly positioned, it is possible to administer the required electron dose and, at the same time, to protect personnel with less shielding than is needed in the prior method. Adequate shielding can be provided by concrete walls 6 ft (≈ 1.8 m) high and 16 in. (≈ 41 cm) thick, without a ceiling.

The success of the present method depends on the use of a cationic epoxy as the matrix material in the prepreg tape,

heating the prepreg tape to a temperature of 50 °C immediately prior to layup, and exposing the workpiece to an electron-beam dose of ≈ 2 Mrad. Experiments have shown that structures fabricated by the present method have the same mechanical properties as those of nominally identical structures fabricated by the prior method with electron beams of 3 to 4 MeV.

*This work was done by Catherine A. Byrne and Alexander Bykanov of Science Research Laboratory, Inc. for Marshall Space Flight Center. Further information is contained in a TSP (see page 1).
MFS-31837*

Aluminum-Alloy-Matrix/Alumina-Reinforcement Composites

Relatively inexpensive, lightweight composite parts could be substitutes for some superalloy parts.

Marshall Space Flight Center, Alabama

Isotropic composites of aluminum-alloy matrices reinforced with particulate alumina have been developed as lightweight, high-specific-strength, less-expensive alternatives to nickel-base and ferrous superalloys. These composites feature a specific gravity of about 3.45 g/cm³ and specific strengths of about 200 MPa/(g/cm³). The room-temperature tensile strength is 100 ksi (689 MPa) and stiffness is 30 Msi (206 GPa). At 500 °F (260 °C), these composites have shown 80 percent retention in strength and 95 percent retention in stiffness. These materials also have excellent fatigue tolerance and tribological properties. They can be fabricated in net (or nearly net) sizes and shapes to make housings, pistons, valves, and ducts in turbomachinery, and to make structural

components of such diverse systems as diesel engines, automotive brake systems, and power-generation, mining, and oil-drilling equipment. Separately, incorporation of these metal matrix composites within aluminum gravity castings for localized reinforcement has been demonstrated.

A composite part of this type can be fabricated in a pressure infiltration casting process. The process begins with the placement of a mold with alumina particulate preform of net or nearly net size and shape in a crucible in a vacuum furnace. A charge of the alloy is placed in the crucible with the preform. The interior of the furnace is evacuated, then the furnace heaters are turned on to heat the alloy above its liquidus temperature. Next, the interior of the furnace is filled

with argon gas at a pressure about 900 psi (≈ 6.2 MPa) to force the molten alloy to infiltrate the preform. Once infiltrated, the entire contents of the crucible can be allowed to cool in place, and the composite part recovered from the mold.

This work was done by Uday Kashalikar and Boris Rozenoyer of Foster-Miller, Inc., for Marshall Space Flight Center.

In accordance with Public Law 96-517, the contractor has elected to retain title to this invention. Inquiries concerning rights for its commercial use should be addressed to:

Foster-Miller, Inc.

350 Second Avenue

Waltham, MA 02451

Telephone No.: (781) 684-4000

Refer to MFS-31784, volume and number of this NASA Tech Briefs issue, and the page number.

Fibrous-Ceramic/Aerogel Composite Insulating Tiles

The best features of aerogels and fibrous ceramics are exploited.

Ames Research Center, Moffett Field, California

Fibrous-ceramic/aerogel composite tiles have been invented to afford combinations of thermal-insulation and mechanical properties superior to those attainable by making tiles of fibrous ceramics alone or aerogels alone. These lightweight tiles can be tailored to a variety of applications that range from insulating cryogenic tanks to protecting spacecraft against re-entry heating.

The advantages and disadvantages of fibrous ceramics and aerogels can be summarized as follows:

- Tiles made of ceramic fibers are known for mechanical strength, toughness, and machinability. Fibrous ceramic tiles are highly effective as thermal insulators in a vacuum. However, undesirably, the porosity of these materials makes them permeable by

gases, so that in the presence of air or other gases, convection and gas-phase conduction contribute to the effective thermal conductivity of the tiles.

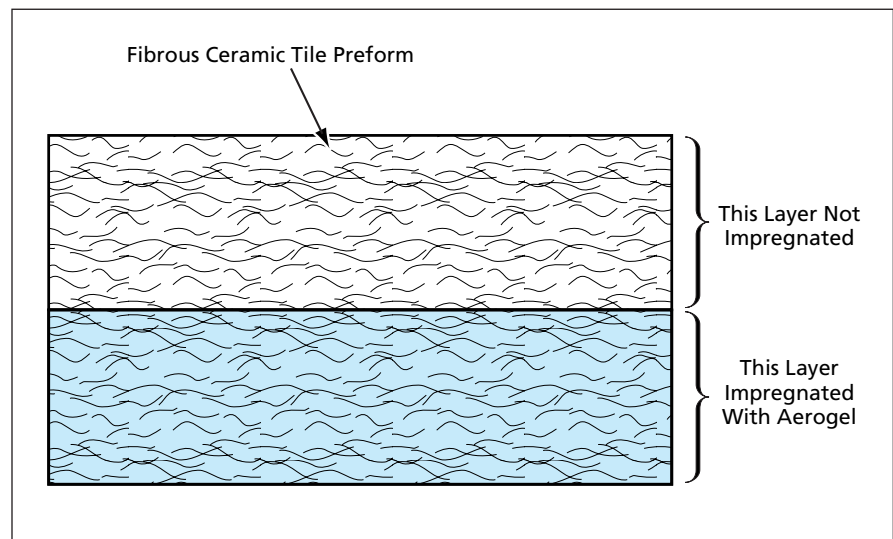
- Other disadvantages of the porosity and permeability of fibrous ceramic tiles arise because gases (e.g., water vapor or cryogenic gases) can condense in pores. This condensation contributes to weight, and in the case

of cryogenic systems, the heat of condensation undesirably adds to the heat flowing to the objects that one seeks to keep cold. Moreover, there is a risk of explosion associated with vaporization of previously condensed gas upon reheating.

- Aerogels offer low permeability, low density, and low thermal conductivity, but are mechanically fragile.

The basic idea of the present invention is to exploit the best features of fibrous ceramic tiles and aerogels. In a composite tile according to the invention, the fibrous ceramic serves as a matrix that mechanically supports the aerogel, while the aerogel serves as a low-conductivity, low-permeability filling that closes what would otherwise be the open pores of the fibrous ceramic. Because the aerogel eliminates or at least suppresses permeation by gas, gas-phase conduction, and convection, the thermal conductivity of such a composite — even at normal atmospheric pressure — is not much greater than that of the fibrous ceramic alone in a vacuum.

In a typical application, a composite tile according to the invention is made from an open-pore rigid ceramic-fiber tile preform by impregnating the preform with an aerogel part way through its thickness (see figure). The details of the impregnation process depend on the specific ceramic and aerogel materi-



A Fibrous Ceramic Tile Preform Is Impregnated with an aerogel part way through its thickness. The invention is not restricted to a single aerogel-impregnated layer as shown here: alternatively, there can be multiple layers impregnated by the same aerogel and/or different aerogels.

als, the desired thickness of the aerogel-impregnated layer, and the desired density of the aerogel. In general, one prepares an aerogel-precursor solution by mixing two component solutions. The preform is partially infiltrated with the precursor solution. The gelation reaction occurs spontaneously between the components of the solution at room temperature. To complete the process, the aerogel is dried in one or more subprocesses that can include fluid extraction at supercritical temperature and

pressure, heating to a temperature above ambient but below the sintering temperature of the aerogel, venting, and/or purging with dry air.

This work was done by Susan M. White and Daniel J. Rasky of Ames Research Center. Further information is contained in a TSP (see page 1).

Inquiries concerning rights for the commercial use of this invention should be addressed to the Patent Counsel, Ames Research Center, (650) 604-5104. Refer to ARC-12070.

Urethane/Silicone Adhesives for Bonding Flexing Metal Parts

These adhesives make strong, flexible bonds.

NASA's Jet Propulsion Laboratory, Pasadena, California

Adhesives that are blends of commercially available urethane and silicone adhesives have been found to be useful for bonding metal parts that flex somewhat during use. These urethane/silicone adhesives are formulated for the specific metal parts to be bonded. The bonds formed by these adhesives have peel and shear strengths greater than those of bonds formed by double-sided tapes and by other adhesives, including epoxies and neat silicones. In addition, unlike the bonds formed by epoxies, the bonds formed by these adhesives retain flexibility.

In the initial application for which the urethane/silicone adhesives were de-

vised, there was a need to bond spring rings, which provide longitudinal rigidity for inflatable satellite booms, with the blades that provide the booms' axial strength. The problem was to make the bonds withstand the stresses, associated with differences in curvature between the bonded parts, that arose when the booms were deflated and the springs were compressed. In experiments using single adhesives (that is, not the urethane/silicone blends), the bonds were broken and, in each experiment, it was found that the adhesive bonded well with either the ring or with the blade, but not both. After numerous experiments, the adhesive that bonded best

with the rings and the adhesive that bonded best with the blades were identified. These adhesives were then blended and, as expected, the blend bonded well with both the rings and the blades.

The two adhesives are Kalex (or equivalent) high-shear-strength urethane and Dow Corning 732 (or equivalent) silicone. The nominal mixture ratio is 5 volume parts of the urethane per 1 volume part of the silicone. Increasing the proportion of silicone makes the bond weaker but more flexible, and decreasing the proportion of silicone makes the bond stronger but more brittle.

The urethane/silicone blend must be prepared and used quickly because

of the limited working time of the urethane: The precursor of the urethane adhesive is supplied in a two-part form, comprising a resin and a hardener that must be mixed. The resulting urethane adhesive has a working time of 3 to 5 minutes. To prepare the urethane/silicone blend, one must quickly add the silicone to the urethane adhesive and mix it in thoroughly within the working time of the urethane.

Once the urethane/silicone blend has been mixed and applied to the bond surfaces, it takes about 2 hours for the adhesive to cure under pressure. However, it takes about 24 hours for the adhesive to reach full strength.

*This work was done by Paul D. Edwards of Caltech for **NASA's Jet Propulsion Laboratory**. Further information is contained in a TSP (see page 1). In accordance with Public Law 96-517, the contractor has elected to retain title to this invention. Inquiries concern-*

ing rights for its commercial use should be addressed to:

*Innovative Technology Assets Management
JPL*

*Mail Stop 202-233
4800 Oak Grove Drive
Pasadena, CA 91109-8099
(818) 354-2240*

E-mail: iaoffice@jpl.nasa.gov

Refer to NPO-30737, volume and number of this NASA Tech Briefs issue, and the page number.



Scalable Architecture for Multihop Wireless *ad Hoc* Networks

These networks could readily be expanded and reconfigured.

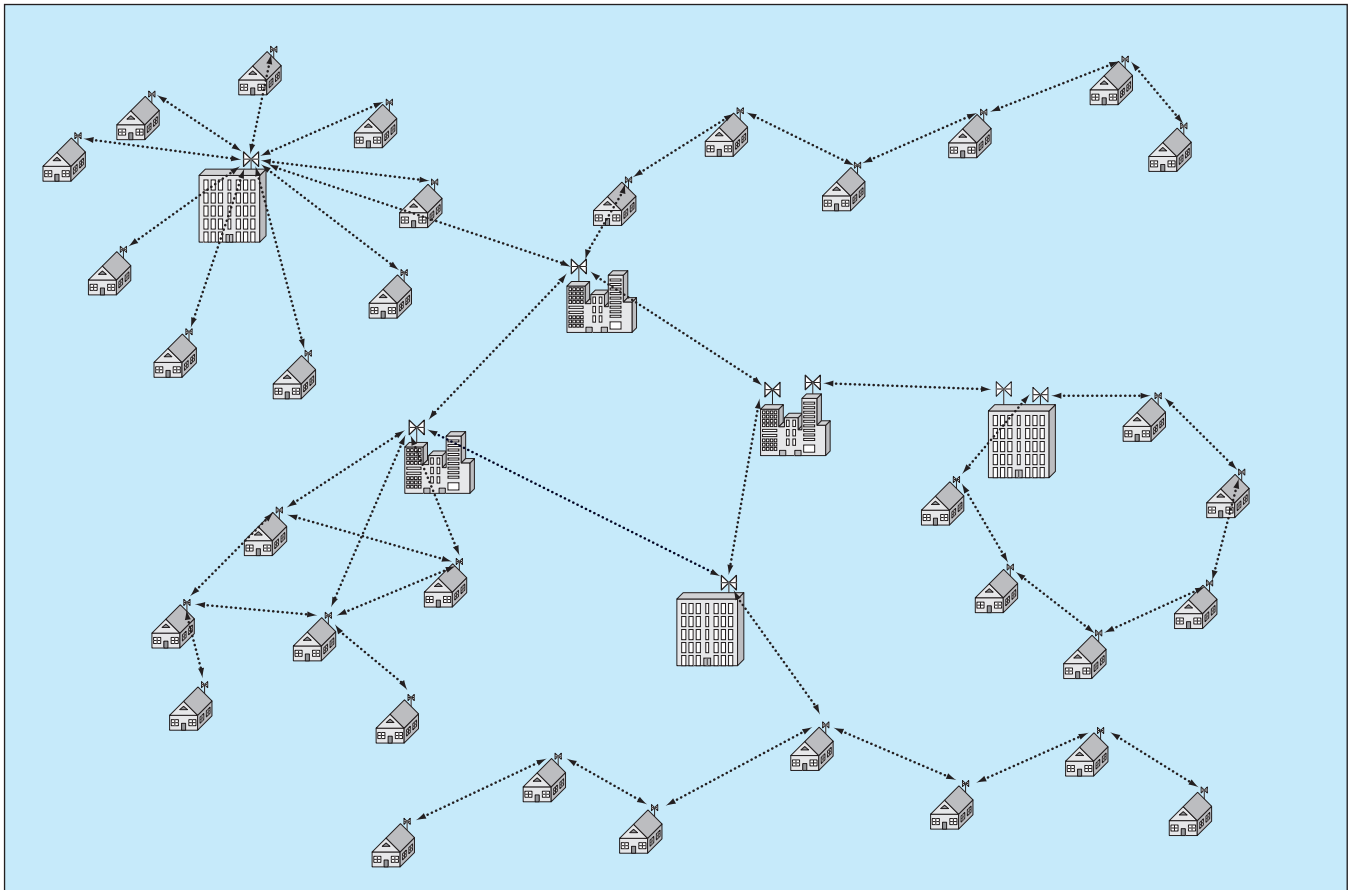
NASA's Jet Propulsion Laboratory, Pasadena, California

A scalable architecture for wireless digital data and voice communications via *ad hoc* networks has been proposed. Although the details of the architecture and of its implementation in hardware and software have yet to be developed, the broad outlines of the architecture are fairly clear: This architecture departs from current commercial wireless communication architectures, which are characterized by low effective bandwidth per user and are not well suited to low-cost, rapid scaling in large metropolitan areas. This architecture is inspired by a vision more akin to that of more than two dozen noncommercial community wireless networking organizations established by volunteers in North America and several European countries.

One of the basic principles of this architecture is that of a hierarchy of net-

works, built on local community networking via shared resources (see figure), with enough flexibility to provide service on demand and to enable growth as the need arises. In the proposed architecture, at least some users' wireless communication units would serve as relay stations for other users' units, enabling any user within the range of another, participating user to gain access to the local- and wider-area networks in a multihop manner. The success of the architecture would depend heavily on the development of an energy-efficient, multihop, *ad hoc* network routing protocol. This would ideally be implemented in reconfigurable hardware to enable dynamic protocol "preferencing," and easy upgrades to potential future wireless protocol standards.

Power-efficient communication would take place by multihop radio at the local level and via high-speed point-to-point links (e.g., fiber, satellite) at the global level. In a typical community, the home of each user would be equipped with a rooftop radio transceiver that, together with a number of neighboring similar units, would be a member of a microcell. Each such unit would be capable of communicating with a central unit of the microcell, either directly or by relay via one of the other members. When at home, a user's telephone, personal digital assistant (PDA), laptop computer with wireless modem, or other communication device would connect with the network via the in-home wireless link and the rooftop transceiver. When out of range of the in-home wireless link, the user would connect to the network



Neighboring Rooftop Radio Transceivers would be grouped into microcells connected via a wireless backbone to build city-wide and higher-level networks.

via someone else's rooftop transceiver, or portable wireless device, in a multi-hop fashion.

Microcells within a community are aggregated into cells by use of a local-area-network (LAN) backbone of higher speed wireless and/or wired connections. Every time a microcell connects to the wireless backbone, microcells or individual users in surrounding blocks can also connect to the network. Repeating this process, a network serving a wider area would be built. At various locations, the wireless traffic would be placed on the Internet backbone.

The proposed architecture is envisioned as extending Moore's law to Internet bandwidth and thereby offering

an economic benefit. Moore's law (which is not really a law but an informal prediction that closely approximates what has been observed in industry) states that the numbers of transistors per unit area in microprocessors double about every 18 months. The consequences of Moore's law include both increasing capacity of the affected equipment and lower per-unit costs. The extension of Moore's law to Internet bandwidth has been estimated to offer the potential to reduce the cost of 1 Mb/s of Internet bandwidth to only \$1 per month after ten years.

This work was done by Payman Arabshahi, Andrew Gray, Clayton Okino, and Tsun-Yee Yan of Caltech for NASA's Jet Propulsion

Laboratory. Further information is contained in a TSP (see page 1).

In accordance with Public Law 96-517, the contractor has elected to retain title to this invention. Inquiries concerning rights for its commercial use should be addressed to:

Intellectual Assets Office

JPL

Mail Stop 202-233

4800 Oak Grove Drive

Pasadena, CA 91109

(818) 354-2240

E-mail: ipgroup@jpl.nasa.gov

Refer to NPO-30452, volume and number of this NASA Tech Briefs issue, and the page number.

Improved Thermoplastic/Iron-Particle Transformer Cores

Proper choice of particle-size distribution results in minimal eddy-current loss.

Langley Research Center, Hampton, Virginia

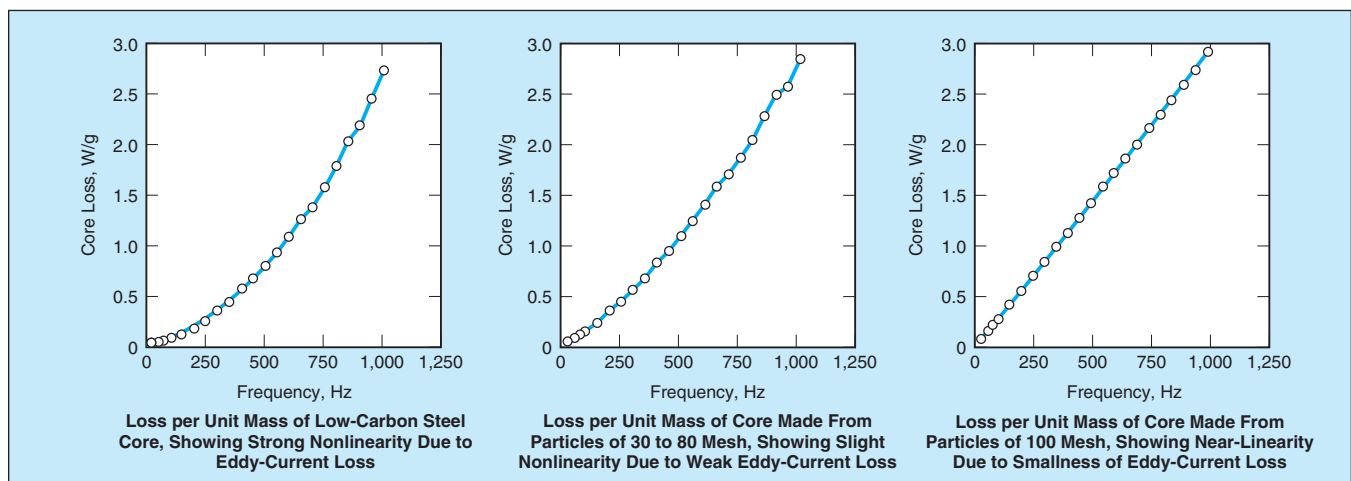
A method of fabricating improved transformer cores from composites of thermoplastic matrices and iron-particles has been invented. Relative to commercially available laminated-iron-alloy transformer cores, the cores fabricated by this method weigh less and are less expensive. Relative to prior polymer-matrix/iron-particle composite-material transformer cores, the cores fabricated by this method can be made mechanically stronger and more magnetically permeable. In addition, whereas some prior cores have exhibited significant eddy-current losses, the cores fabricated by this method exhibit very small eddy-current losses. The cores made by this

method can be expected to be attractive for use in diverse applications, including high-signal-to-noise transformers, stepping motors, and high-frequency ignition coils.

The present method is a product of an experimental study of the relationships among fabrication conditions, final densities of iron particles, and mechanical and electromagnetic properties of fabricated cores. Among the fabrication conditions investigated were molding pressures (83, 104, and 131 MPa), and molding temperatures (250, 300, and 350 °C). Each block of core material was made by uniaxial-compression molding, at the applicable pressure/temperature

combination, of a mixture of 2 weight percent of LaRCT™ (or equivalent high-temperature soluble thermoplastic adhesive) with 98 weight percent of approximately spherical iron particles having diameters in the micron range. Each molded block was cut into square-cross-section rods that were used as core specimens in mechanical and electromagnetic tests. Some of the core specimens were annealed at 900 °C and cooled slowly before testing. For comparison, a low-carbon-steel core was also tested.

The results of the tests showed that density, hardness, and rupture strength generally increased with molding pres-



The **Total Losses as Functions of Frequency** were measured in three cores at a magnetic induction of 5 kilogauss (0.5 Tesla). In general, the total frequency-dependent loss in a given core is the sum of a linear hysteresis contribution and a quadratic eddy-current contribution. Hence, the near-linearity of the curve in the 100-mesh case is evidence of low eddy-current loss.

sure and temperature, though the correlation was rather weak. The weakness of the correlation was attributed to the pores in the specimens. The maximum relative permeabilities of cores made without annealing ranged from 30 to 110, while those of cores made with annealing ranged from 900 to 1,400. However, the greater permeabilities of the

annealed specimens were not associated with noticeably greater densities.

The major practical result of the investigation was the discovery of an optimum distribution of iron-particle sizes: It was found that eddy-current losses in the molded cores were minimized by using 100 mesh (corresponding to particles with diameters $\leq 100 \mu\text{m}$) iron par-

ticles. The effect of optimization of particle sizes on eddy-current losses is depicted in the figure.

*This work was done by Russell A. Winch-
eski, Robert G. Bryant, and Min Namkung of
Langley Research Center. Further informa-
tion is contained in a TSP (see page 1).
LAR-15719*

Cooperative Lander-Surface/Aerial Microflyer Missions for Mars Exploration

Bio-inspired principles of key functions are distilled, enabling missions to Mars using multiple microflyers in synergy with the existing surface assets to provide a robust telecommunication architecture for gathering scientific data.

NASA's Jet Propulsion Laboratory, Pasadena, California

Concepts are being investigated for exploratory missions to Mars based on "Bioinspired Engineering of Exploration Systems" (BEES), which is a guiding principle of this effort to develop biomorphic explorers. The novelty lies in the use of a robust telecom architecture for mission data return, utilizing multiple local relays (including the lander itself as a local relay and the explorers in the dual role of a local relay) to enable ranges ~ 10 to 1,000 km and downlink of color imagery. As illustrated in Figure 1, multiple microflyers that can be both surface or aerially launched are envisioned in shepherding, metamorphic, and imaging roles. These microflyers imbibe key bio-inspired principles in their flight control, navigation, and visual search operations. Honey-bee inspired algorithms utilizing visual cues to perform autonomous navigation operations such as terrain following will be utilized. The instrument suite will consist of a panoramic imager and polarization imager specifically optimized to detect ice and water. For microflyers, particularly at small sizes, bio-inspired solutions appear to offer better alternate solutions than conventional engineered approaches.

This investigation addresses a wide range of interrelated issues, including desired scientific data, sizes, rates, and communication ranges that can be accomplished in alternative mission scenarios.

The mission illustrated in Figure 1 offers the most robust telecom architecture and the longest range for exploration with two landers being available as main local relays in addition to an ephemeral aerial probe local relay. The shepherding or metamorphic plane are in their

dual role as local relays and image data collection/storage nodes. Appropriate placement of the landing site for the scout lander with respect to the main mission lander can allow coverage of extremely large ranges and enable exhaustive survey of the area of interest. In particular, this mission could help with the path planning and risk mitigation in the traverse of the long-distance surface explorer/rover. The basic requirements of design and operation of BEES to implement the scenarios are discussed. Terrestrial applications of such concepts include distributed aerial/surface measurements of meteorological events, i.e., storm watch, seismic monitoring, reconnaissance, biological chemical sensing, search and rescue, surveillance, autonomous security/protection agents, and/or delivery of agents (sensors, surface/sub-surface crawlers, clean-up agents). Figure 2 illustrates an Earth demonstration that is in development, and its implementation will illustrate the value of these biomorphic mission concepts.

*This work was done by Sarita Thakoor and Norman Lay of Caltech for NASA's Jet Propulsion Laboratory and Butler Hine and Steven Zornetzer of Ames Research Center for the NASA Intelligent Systems Program. Further information is contained in a TSP (see page 1).
NPO-30286*

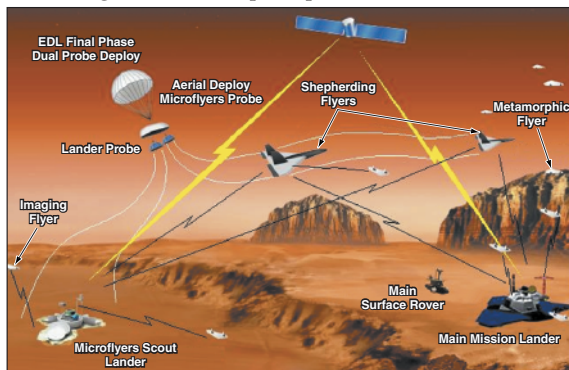


Figure 1: A **Biomorphic Mars Mission** is conceptualized here. (Note: EDL= Entry, Descent, and Landing.)

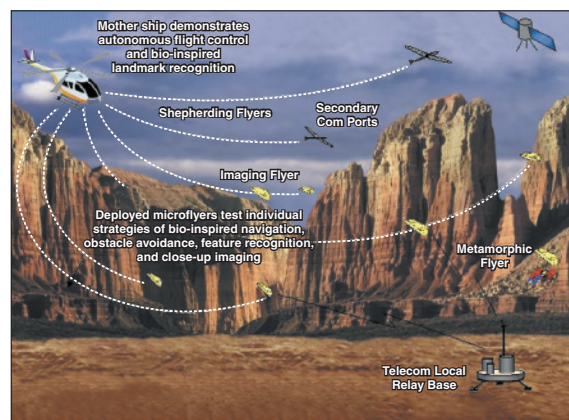


Figure 2: This is a **Conceptual Illustration of a Planned Demonstration**, "Bioinspired Engineering of Exploration Systems for MARS," to be performed at a MARS analog site on Earth. Here, microflyers work in synergy with the existing surface/aerial systems to enable new science endeavors. Multiple local comports provide a robust communication route for imagery downlink from the microflyers.

Dual-Frequency Airborne Scanning Rain Radar Antenna System

Spatially coincident horizontally and vertically polarized beams are generated at both frequencies.

NASA's Jet Propulsion Laboratory, Pasadena, California

A compact, dual-frequency, dual-polarization, wide-angle-scanning antenna system has been developed as part of an airborne instrument for measuring rainfall. This system is an

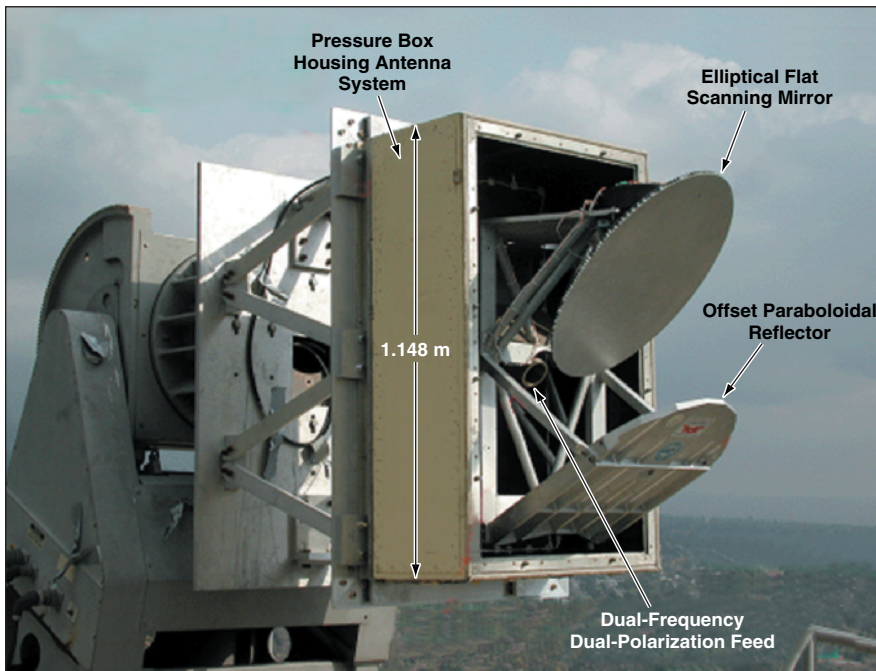
upgraded version of a prior single-frequency airborne rain radar antenna system and was designed to satisfy stringent requirements. One particularly stringent combination of require-

ments is to generate two dual-polarization (horizontal and vertical polarizations) beams at both frequencies (13.405 and 35.605 GHz) in such a way that the beams radiated from the antenna point in the same direction, have 3-dB angular widths that match within 25 percent, and have low side-lobe levels over a wide scan angle at each polarization-and-frequency combination. In addition, the system is required to exhibit low voltage standing-wave ratios at both frequencies.

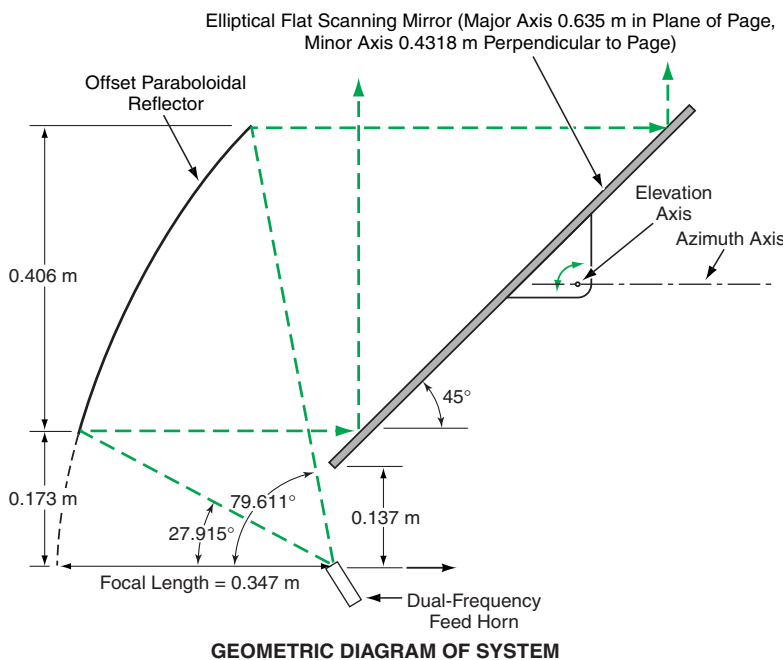
The system (see figure) includes a flat elliptical scanning reflector and a stationary offset paraboloidal reflector illuminated by a common-aperture feed system that comprises a corrugated horn with four input ports — one port for each of the four frequency-and-polarization combinations. The feed horn is designed to simultaneously (1) under-illuminate the reflectors 35.605 GHz and (2) illuminate the reflectors with a 15-dB edge taper at 13.405 GHz. The scanning mirror is rotated in azimuth to scan the antenna beam over an angular range of $\pm 20^\circ$ in the cross-track direction for wide swath coverage, and in elevation to compensate for the motion of the aircraft.

The design of common-aperture feed horn makes it possible to obtain the required absolute gain and low side-lobe levels in wide-angle beam scanning. The combination of the common-aperture feed horn with the small (0.3) focal-length-to-diameter ratio of the paraboloidal reflector makes it possible for the overall system to be compact enough that it can be mounted on a DC-8 airplane. The input ports are oriented orthogonally and carefully positioned and the depths of the corrugations in the feed horn were chosen carefully, all in an effort to minimize the overall level of cross-polarization and side-lobe level in the system.

For optimum performance, the feed phase center would ordinarily be kept at the focal point of the offset paraboloidal reflector. It would be possible to do so in single-frequency operation, but it is not possible to have a single feed phase center for both of the widely separated frequencies of this system. Instead, the feed horn is designed so that the combination



SYSTEM POSITIONED FOR MEASUREMENTS AT AN ANTENNA-TESTING RANGE



GEOMETRIC DIAGRAM OF SYSTEM

This Airborne Rain Radar Antenna System includes a flat scanning reflector fed by an offset paraboloidal reflector fed by a single feed horn with four ports. Each feed port handles one of four frequency-and-polarization combinations.

of locations is optimal in the sense that it yields an optimal combination of gains, matched 3-dB widths, low cross-polarization, and low side-lobe levels. The elliptical shape of the scanning mirror was cho-

sen, from among a number of superquadric shapes, as the one that results in the lowest overall side-lobe levels.

This work was done by Ziad A. Hussein of Caltech and Ken Green of Microwave Engi-

neering Corp. for NASA's Jet Propulsion Laboratory. Further information is contained in a TSP (see page 1). NPO-30506

Eight-Channel Continuous Timer

This timer measures every cycle of every input clock signal.

NASA's Jet Propulsion Laboratory, Pasadena, California

A custom laboratory electronic timer circuit measures the durations of successive cycles of nominally highly stable input clock signals in as many as eight channels, for the purpose of statistically quantifying the small instabilities of these signals. The measurement data generated by this timer are sent to a personal computer running software that integrates the measurements to form a phase residual for each channel and uses the phase residuals to compute Allan variances for each channel. (The Allan variance is a standard statistical measure of instability of a clock signal.) Like other laboratory clock-cycle-measuring circuits, this timer utilizes an externally generated reference clock signal having a known frequency (100 MHz) much higher than the frequencies of the input clock signals (between 100 and 120 Hz). It counts the number of reference-clock cycles that occur between successive rising edges

of each input clock signal of interest, thereby affording a measurement of the input clock-signal period to within the duration (10 ns) of one reference clock cycle. Unlike typical prior laboratory clock-cycle-measuring circuits, this timer does not skip some cycles of the input clock signals. The non-cycle-skipping feature is an important advantage because in applications that involve integration of measurements over long times for characterizing nominally highly stable clock signals, skipping cycles can degrade accuracy.

The timer includes a field-programmable gate array that functions as a 20-bit counter running at the reference clock rate of 100 MHz. The timer also includes eight 20-bit latching circuits — one for each channel — at the output terminals of the counter. Each transition of an input signal from low to high causes the corresponding latching circuit to latch

the count at that instant. Each such transition also sets a status flip-flop circuit to indicate the presence of the latched count. A microcontroller reads the values of all eight status flip-flops and then reads the latched count for each channel for which the flip-flop indicates the presence of a count. Reading the count for each channel automatically causes the flip-flop of that channel to be reset. The microcontroller places the counts in time order, identifies the channel number for each count, and transmits these data to the personal computer.

This work was done by Steven Cole of Caltech for NASA's Jet Propulsion Laboratory. Further information is contained in a TSP (see page 1).

The software used in this innovation is available for commercial licensing. Please contact Don Hart of the California Institute of Technology at (818) 393-3425. Refer to NPO-40233.

Reduction of Phase Ambiguity in an Offset-QPSK Receiver

Ambiguity would be reduced to twofold at no cost in power efficiency.

NASA's Jet Propulsion Laboratory, Pasadena, California

Proposed modifications of an offset-quadrature-phase-shift keying (offset-QPSK) transmitter and receiver would reduce the amount of signal processing that must be done in the receiver to resolve the QPSK fourfold phase ambiguity. Resolution of the phase ambiguity is necessary in order to synchronize with the received carrier signal, the signal generated by a local oscillator in a carrier-tracking loop in the receiver. Without resolution of the fourfold phase ambiguity, the loop could lock to any of four possible phase points, only one of which has the proper phase relationship with the carrier.

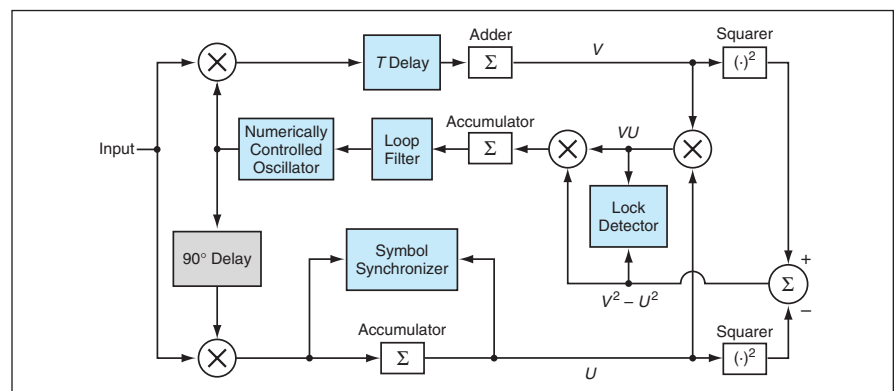


Figure 1. This **Carrier-Tracking Loop** of an offset-QPSK receiver differs from a maximum a posteriori (MAP) carrier-tracking loop of a non-offset-QPSK receiver by incorporating a unit that imposes a delay of one symbol period (T).

The proposal applies, more specifically, to an offset-QPSK receiver that contains a carrier-tracking loop like that shown in Figure 1. This carrier-tracking loop does not resolve or reduce the phase ambiguity. A carrier-

tracking loop of a different design optimized for the reception of offset QPSK could reduce the phase ambiguity from fourfold to twofold, but would be more complex. Alternatively, one could resolve the fourfold phase ambiguity by

use of differential coding in the transmitter, at a cost of reduced power efficiency. The proposed modifications would make it possible to reduce the fourfold phase ambiguity to twofold, with no loss in power efficiency and only relatively simple additional signal-processing steps in the transmitter and receiver. The twofold phase ambiguity would then be resolved by use of a unique synchronization word, as is commonly done in binary phase-shift keying (BPSK).

Although the mathematical and signal-processing principles underlying the modifications are too complex to explain in detail here, the modifications themselves would be relatively simple and are best described with the help of simple block diagrams (see Figure 2). In the transmitter, one would add a unit that would periodically invert bits going into the QPSK modulator; in the receiver, one would add a unit that would effect different but corresponding inversions of bits coming out of the QPSK demodulator. The net effect of all the inversions would be that depending on which lock point the carrier-tracking loop had selected, all the output bits would be either inverted or non-inverted together; hence, the ambiguity would be reduced from fourfold to twofold, as desired.

This work was done by Jeff Berner and Peter Kinman of Caltech for NASA's Jet Propulsion Laboratory. Further information is contained in a TSP (see page 1). NPO-30384

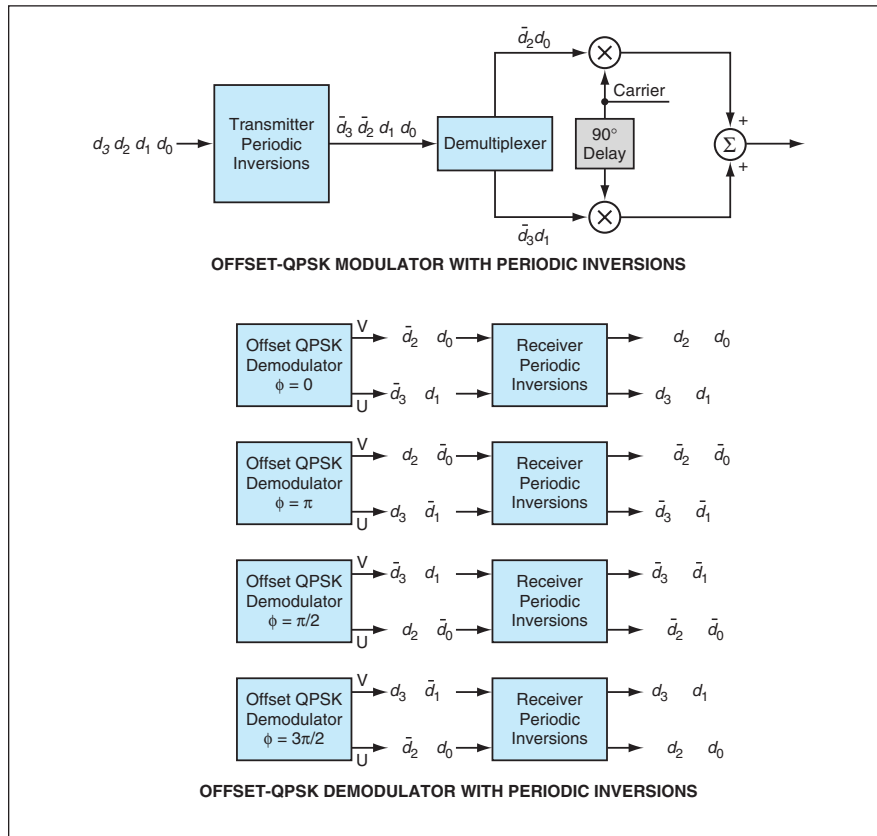


Figure 2. Inversions of Bits in cycles of four bits ($d_0 d_1 d_2 d_3$) would cause all the output bits to be either inverted or noninverted together, depending on the phase difference (ϕ) between the received carrier and the local-oscillator signal in the carrier-tracking loop. The loop could lock at any of four points ($\phi = 0, \pi/2, \pi, \text{ or } 3\pi/2$ radians).

Ambient-Light-Canceling Camera Using Subtraction of Frames

Ambient light would be suppressed more effectively than by optical filtering alone.

NASA's Jet Propulsion Laboratory, Pasadena, California

The ambient-light-canceling camera (ALCC) is a proposed near-infrared electronic camera that would utilize a combination of (1) synchronized illumination during alternate frame periods and (2) subtraction of readouts from consecutive frames to obtain images without a background component of ambient light. The ALCC is intended especially for use in tracking the motion of an eye by the pupil center corneal reflection (PCCR) method. Eye tracking by the PCCR method has shown potential for application in human-computer interaction for people with and without disabilities, and

for noninvasive monitoring, detection, and even diagnosis of physiological and neurological deficiencies.

In the PCCR method, an eye is illuminated by near-infrared light from a light-emitting diode (LED). Some of the infrared light is reflected from the surface of the cornea. Some of the infrared light enters the eye through the pupil and is reflected from back of the eye out through the pupil — a phenomenon commonly observed as the “red-eye” effect in flash photography. An electronic camera is oriented to image the user's eye. The output of the camera is digitized and processed by algorithms that

locate the two reflections. Then from the locations of the centers of the two reflections, the direction of gaze is computed. As described thus far, the PCCR method is susceptible to errors caused by reflections of ambient light. Although a near-infrared band-pass optical filter can be used to discriminate against ambient light, some sources of ambient light have enough in-band power to compete with the LED signal.

The mode of operation of the ALCC would complement or supplant spectral filtering by providing more nearly complete cancellation of the effect of ambient light. In the operation of the ALCC,

a near-infrared LED would be pulsed on during one camera frame period and off during the next frame period. Thus, the scene would be illuminated by both the LED (signal) light and the ambient (background) light during one frame period, and would be illuminated with only ambient (background) light during the next frame period. The camera output would be digitized and sent to a computer, wherein the pixel values of the background-only frame would be subtracted from the pixel values of the signal-plus-background frame to obtain

signal-only pixel values (see figure).

To prevent artifacts of motion from entering the images, it would be necessary to acquire image data at a rate greater than the standard video rate of 30 frames per second. For this purpose, the ALCC would exploit a novel control technique developed at NASA's Jet Propulsion Laboratory for advanced charge-coupled-device (CCD) cameras. This technique provides for readout from a subwindow [region of interest (ROI)] within the image frame. Because the desired reflections from the eye would typically occupy a small fraction

of the area within the image frame, the ROI capability would make it possible to acquire and subtract pixel values at rates of several hundred frames per second — considerably greater than the standard video rate and sufficient to both (1) suppress motion artifacts and (2) track the motion of the eye between consecutive subtractive frame pairs.

This work was done by John Michael Moorokian of Caltech for NASA's Jet Propulsion Laboratory. Further information is contained in a TSP (see page 1). NPO-30875

Lightweight, Flexible, Thin, Integrated Solar-Power Packs

These systems could be attractive alternatives to conventional solar arrays and associated power circuits.

Lyndon B. Johnson Space Center, Houston, Texas

Lightweight, flexible, thin, one-piece, solar-power packs are undergoing development. Each power pack of this type is a complete, modular, integrated power-supply system comprising three power subsystems that, in conventional practice, have been constructed as separate units and connected to each other by wires. These power packs are amenable to a variety of uses: For example, they could be laminated to the tops of tents and other shelters to provide or augment power for portable electronic equipment in the field, and they could be used as power sources for such small portable electronic systems as radio transceivers (including data relays and cellular telephones), laptop computers, video camcorders, and Global Positioning System receivers.

The three power subsystems in question are (1) an array of one or more photovoltaic cells (power-generation subsystem), (2) one or more storage batteries (energy-storage subsystem), and (3) electronic circuits to control the other two subsystems and the overall operation of the system [power-management-and-distribution (PMAD) subsystem]. The conventional approach to designing these subsystems results in impediments to the present goal of developing a highly integrated system: Conventional photo-

voltic arrays are fragile and expensive; conventional storage batteries are bulky, must typically be able to withstand high pressures, and must be kept within fairly narrow ranges of operating temperatures; and conventional PMAD systems comprise high-power centralized conditioning and switching circuits that are formed on heavy, rigid printed-circuit boards and generate large amounts of waste heat. The structural, electrical, and thermal requirements that govern the design of a conventional power system usually make it necessary to mount each subsystem in a different location. For example, a photovoltaic array must be placed where it can face the Sun, the storage batteries must be mounted on a wall that can be kept at an acceptable temperature, and the PMAD subsystem must be mounted on a panel suitable for electronic circuitry.

A system of the type under development differs from a conventional power system in several notable ways:

- The power-generation subsystem is based on copper indium gallium diselenide (CIGS), which is a photovoltaic material well suited for flexible, thin-film photovoltaic cells and arrays. In comparison with conventional silicon-based photovoltaic arrays, thin-film

CIGS photovoltaic arrays offer potential advantages of flexibility, durability, high specific power, and low cost.

- The energy-storage subsystem consists mainly of flexible, thin-film lithium-based storage batteries. These are durable batteries that exploit long-life solid-state chemistry and can operate over a wide temperature range.
- The PMAD subsystem is implemented in thin, flexible electronic circuitry instead of conventional circuitry on rigid circuit boards.
- The integrated system can be made by laminating the three thin subsystems and forming vias (through-the-thickness electrical connections) among them.
- The weight and volume of the integrated system are much less than those of an equivalent conventional system that comprises three separate, wire-connected subsystems.
- Duplicates of the system, regarded as modules, can be combined into larger systems to satisfy larger power demands.

This work was done by Robert R. Hanson of ITN Energy Systems, Inc., for Johnson Space Center. Further information is contained in a TSP (see page 1). MSC-23007

Windows®-Based Software Models Cyclic Oxidation Behavior

Oxidation of high-temperature aerospace materials is a universal issue for combustion-path components in turbine or rocket engines. In addition to the question of the consumption of material due to growth of protective scale at use temperatures, there is also the question of cyclic effects and spallation of scale on cooldown. The spallation results in the removal of part of the protective oxide in a discontinuous step and thereby opens the way for more rapid oxidation upon reheating. In experiments, cyclic oxidation behavior is most commonly characterized by measuring changes in weight during extended time intervals that include hundreds or thousands of heating and cooling cycles. Weight gains occurring during isothermal scale-growth processes have been well characterized as being parabolic or nearly parabolic functions of time because diffusion controls reaction rates. In contrast, the net weight change in cyclic oxidation is the sum of the effects of the growth and spallation of scale. Typically, the net weight gain in cyclic oxidation is determined only empirically (that is, by measurement), with no unique or straightforward mathematical connection to either the rate of growth or the amount of metal consumed. Thus, there is a need for mathematical modeling to infer spallation mechanisms.

COSP is a computer program that models the growth and spallation processes of cyclic oxidation on the basis of a few elementary assumptions that were discussed in "COSP: A Computer Model of Cyclic Oxidation," *Oxidation of Metals*, vol. 36, numbers 1 and 2, 1991, pages 81-112. Inputs to the model include the selection of an oxidation-growth law and a spalling geometry, plus oxide-phase, growth-rate, cycle-duration, and spall-constant parameters. (The spalling fraction is often shown to be a constant factor times the existing amount of scale.) The output of COSP includes the net change in weight, the amounts of retained and spalled oxide, the total amounts of oxygen and metal consumed, and the terminal rates of weight loss and metal consumption.

COSP was made publicly available as a DOS-based program in 1991. The present version is a very user-friendly, object-ori-

ented, Windows®-based program, described in "COSP for Windows: Strategies for Rapid Analyses of Cyclic Oxidation Behavior," NASA/TP-2002-211108, February 2002. The present version of COSP can be operated conveniently, while other application programs remain open, for the purpose of (a) importing experimental weight-change data, (b) storing model output data, or (c) plotting model curves. The program affords options for saving and printing information and includes a help file. Point-and-click operating features include multiple drop-down menus for input parameters, importing data, and quick generation of on-screen plots.

One of the displays generated by the program is a plot window that can show, for example, the net-weight-change curve of a chosen model. One can select from among a number of input parameters and mechanisms by tabbing down through a sequence of options, culminating with an "Okay run model" button. Plots for as many as 10 models can be displayed simultaneously for any one of six different output-parameter selections.

Another display generated by the program is a results window, which presents a summary text and a tabulated list of the calculated results. The summary text lists characteristic parameters that are helpful in describing cyclic behavior: such parameters include the maximum weight change, the number of cycles to reach maximum or zero weight, the final rate of weight loss and the fraction of scale spalled on each cycle. The table lists the calculated values for any number of outputs, for every cycle, every 10 cycles, or every 100 cycles. By use of a "copy" spreadsheet button, these tables can be pasted in other spreadsheet or plotting application programs for final storage or presentation.

This program is intended to serve as a software tool for rapidly obtaining a realistic best fit to experimental data for a given oxide type, cycle duration, growth rate, and spalling mechanism. From such a best fit, estimates of the operative parabolic-growth constant and spall constant can be easily extracted. These constants are the only two parameters that are needed to describe well-behaved cyclic oxidation according to a single specified mechanism. The program also makes it possible to estimate the total amount of material consumed by the combined oxidation and spalling process. Another

benefit afforded by this program is to serve as a convenient means to observe the functional behavior of cyclic oxidation curves for any of the various input parameters — for example, by comparing families of curves corresponding to increasing values of one input parameter.

This program was developed by J. L. Smialek and J. V. Auping of Glenn Research Center. Further information is contained in a TSP (see page 1).

Inquiries concerning rights for the commercial use of this invention should be addressed to NASA Glenn Research Center, Commercial Technology Office, Attn: Steve Fedor, Mail Stop 4-8, 21000 Brookpark Road, Cleveland, Ohio 44135. Refer to LEW-17191.

Software for Analyzing Sequences of Flow-Related Images

Spotlight is a computer program for analysis of sequences of images generated in combustion and fluid physics experiments. Spotlight can perform analysis of a single image in an interactive mode or a sequence of images in an automated fashion. The primary type of analysis is tracking of positions of objects over sequences of frames. Features and objects that are typically tracked include flame fronts, particles, droplets, and fluid interfaces. Spotlight automates the analysis of object parameters, such as centroid position, velocity, acceleration, size, shape, intensity, and color. Images can be processed to enhance them before statistical and measurement operations are performed. An unlimited number of objects can be analyzed simultaneously. Spotlight saves results of analyses in a text file that can be exported to other programs for graphing or further analysis. Spotlight is a graphical-user-interface-based program that at present can be executed on Microsoft Windows and Linux operating systems. A version that runs on Macintosh computers is being considered.

This program was written by Robert Klimek and Ted Wright of Glenn Research Center. Further information is contained in a TSP (see page 1).

Inquiries concerning rights for the commercial use of this invention should be addressed to NASA Glenn Research Center, Commercial Technology Office, Attn: Steve Fedor, Mail Stop 4-8, 21000 Brookpark Road, Cleveland Ohio 44135. Refer to LEW-17407



Improved Ball-and-Socket Docking Mechanism

A docking cone and a preload/ejection mechanism would be added to enhance functionality.

Marshall Space Flight Center, Alabama

A proposed docking mechanism would form a ball-and-socket joint in the docked condition. The mechanism could tolerate significant initial misalignment because it would include an alignment cone that would guide the ball into the socket. Like other ball-and-socket joints, the joint would have three rotational degrees of freedom. This docking mechanism would be a successor to the one described in "Passive Capture Joint With Three Degrees of Freedom" (MFS-31146), *NASA Tech Briefs*, Vol. 22, No. 7 (July 1998), page 65. It would contain most of the components of the prior mechanism, plus some additional components that would expand its capabilities.

Like the prior mechanism, the proposed mechanism would comprise two assemblies, which are now denoted the target ball assembly and the socket assembly (see figure). Each assembly would be a part of one of the two vehicles or other objects to be docked with each other. As before, the socket assembly would contain all the moving parts except the target ball. The socket would include the alignment cone, which would taper down to a central cylindrical bore ending in a cup. The bore and cup would be dimensioned to receive the target ball.

As before, the socket assembly would include three locking balls, smaller than the target ball, that would reside in cylindrical holes that would be bored at an angle to the cylindrical axis and that would penetrate the wall of the central cylindrical bore. As before, the locking balls would be spring-loaded against hard stops on a ring and the geometry of the ring and holes would be such as to allow the balls to intrude part way into the central cylindrical bore.

When the target ball was inserted in the socket and pushed toward the cup, it would push the locking balls out of the way, against their spring loads. As the target ball came to a stop in the cup, the springs would once again push the locking balls inward against their hard stops, so that the locking balls

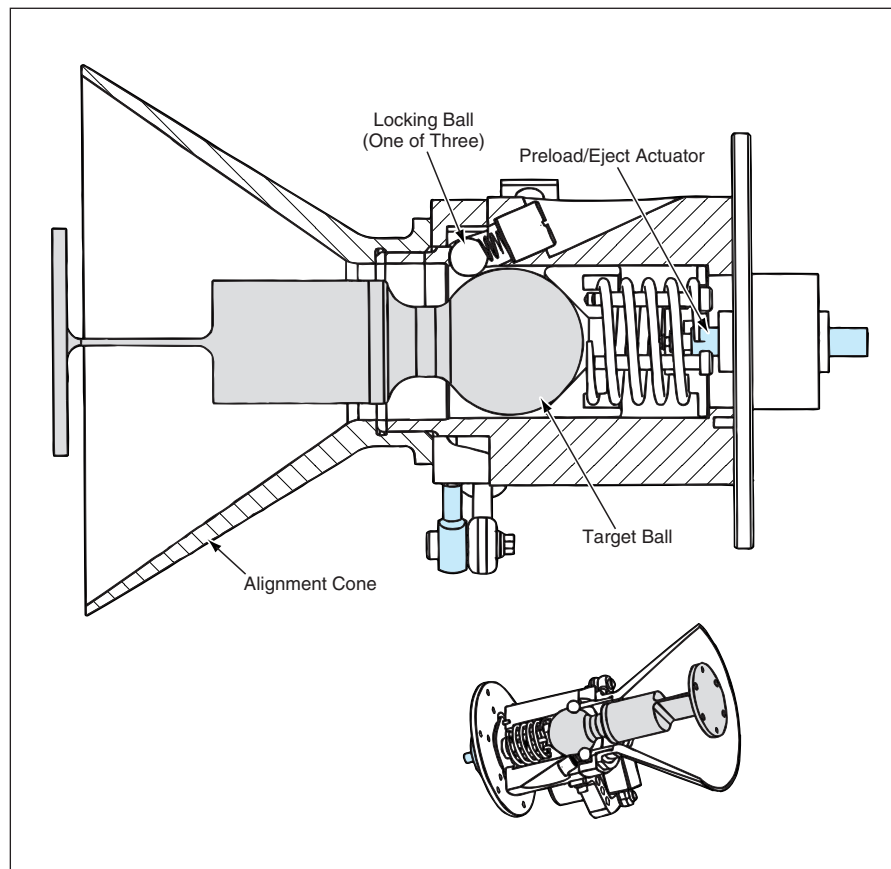
would intrude into the cavity behind the target ball. After this, any attempt to pull the target ball out of the socket would cause the target ball to push the locking balls against their hard stops. The angles of the various surfaces in contact would be such that the net forces would not push the locking balls out of the way and, instead, would lock the balls in place even harder. Thus, the target ball could not be pulled out of the socket.

The proposed mechanism would include a preload/ejection actuator that was not part of the prior docking mechanism. Once the target ball was latched in behind the locking balls, this actuator would push a spring axially against the target ball to preload it against the locking balls and thereby eliminate any axial play in the ball joint. Like the

prior mechanism, the proposed mechanism would include an unlocking actuator that would move the hard stops away from the locking balls to make it possible for the target ball to push the locking balls out of the way and move out of the socket. Once the locking balls were unlocked by the unlocking actuator, the preload/ejection actuator would push the target ball out of the socket.

This work was done by Richard Cloyd and Tom Bryan of Marshall Space Flight Center. Further information is contained in a TSP (see page 1).

This invention is owned by NASA, and a patent application has been filed. For further information, contact Sammy Nabors, MSFC Commercialization Assistance Lead, at sammy.a.nabors@nasa.gov. Refer to MFS-31616.



This **Ball-and-Socket Docking Mechanism** would tolerate large initial misalignment and would be simple and robust, in comparison to prior such mechanisms.

Two-Stage Solenoid

This solenoid would include three cores instead of one.

Marshall Space Flight Center, Alabama

A proposed design for a solenoid-based electromechanical actuator would provide greater starting force than does a comparable conventional design. As used here, “starting force” signifies the magnetic force exerted by the actuator at one end of its stroke when the gap in its magnetic circuit is the widest.

A solenoid of conventional design exerts a large force when its gap is closed. The magnetic force decreases as the gap increases. Hence, typically, the starting force exerted by a conven-

tional solenoid is small; depending upon the specific application, the starting force may even be insufficient to initiate closure.

Whereas a conventional solenoid design provides for only one core, the proposed design calls for three cores, two of these being fixed to one another with a separate core between these two. Analysis shows that in comparison with conventional solenoids, the solenoids of the proposed design would not have a cost impact, could have longer operational

lives, and exhibit larger forces in an open position. It was also reported that the proposed design could be extended to multiple-staged solenoid design, which would yield increased force in the middle of the stroke as well.

This work was done by Jeremy Myers of Marshall Space Flight Center and Frank Speckhart of the University of Tennessee. For further information, contact Sammy Nabors, MSFC Commercialization Assistance Lead, at sammy.a.nabors@nasa.gov. MFS-31923

Ordered Nanostructures Made Using Chaperonin Polypeptides

This method exploits the ability of chaperonins to assemble into complex structures.

Ames Research Center, Moffett Field, California

A recently invented method of fabricating periodic or otherwise ordered nanostructures involves the use of chaperonin polypeptides. The method is intended to serve as a potentially superior and less expensive alternative to conventional lithographic methods for use in the patterning steps of the fabrication of diverse objects characterized by features of the order of nanometers. Typical examples of such objects include arrays of quantum dots that would serve as the functional building blocks of future advanced electronic and photonic devices.

A chaperonin is a double-ring protein structure having a molecular weight of about 60 ± 5 kilodaltons. In nature, chaperonins are ubiquitous, essential, subcellular structures. Each natural chaperonin molecule comprises 14, 16, or 18 protein subunits, arranged as two stacked rings approximately 16 to 18 nm tall by approximately 15 to 17 nm wide, the exact dimensions depending on the biological species in which it originates. The natural role of chaperonins is unknown, but they are believed to aid in the correct folding of other proteins, by en-

closing unfolded proteins and preventing nonspecific aggregation during assembly.

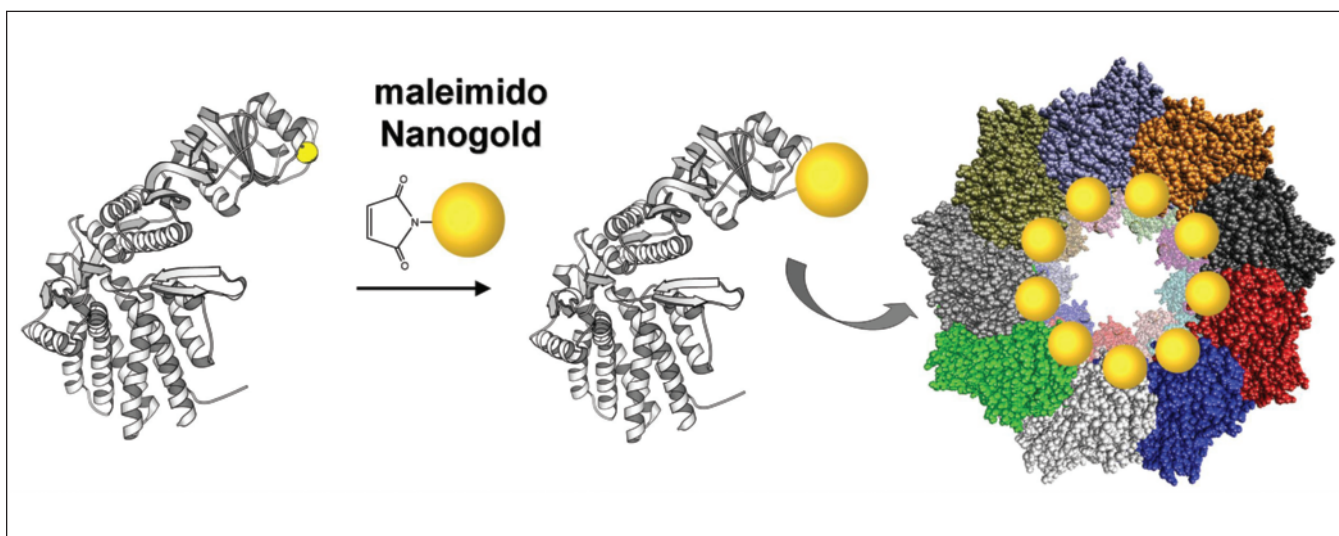
What makes chaperonins useful for the purpose of the present method is that under the proper conditions, chaperonin rings assemble themselves into higher-order structures. This method exploits such higher-order structures to define nanoscale devices. The higher-order structures are tailored partly by choice of chemical and physical conditions for assembly and partly by using chaperonins that have been mutated. The mutations are made by established biochemical techniques.

The assembly of chaperonin polypeptides into such structures as rings, tubes, filaments, and sheets (two-dimensional crystals) can be regulated chemically. Rings, tubes, and filaments of some chaperonin polypeptides can, for example, function as nanovessels if they are able to absorb, retain, protect, and release gases or chemical reagents, including reagents of medical or pharmaceutical interest. Chemical reagents can be bound in, or released from, such structures under suitable controlled conditions.

In an example of a contemplated application, a two-dimensional crystal of chaperonin polypeptides would be formed on a surface of an inorganic substrate and used to form a planar array of nanoparticles or quantum dots. Through genetic engineering of the organisms used to manufacture the chaperonins, specific sites on the chaperonin molecules and, thus, on the two-dimensional crystals can be chemically modified to react in a specific manner so as to favor the deposition of the material of the desired nanoparticles or quantum dots. A mutation that introduces a cysteine residue at the desired sites on a chaperonin of *Sulfolobus shibatae* was used to form planar arrays of gold nanoparticles (see figure).

This work was done Jonathan Trent, Robert McMillan, and Chad Paavola of Ames Research Center; Rakesh Mogul of University of California, Santa Cruz; and Hiromi Kagawa of SETI Institute. For further information, access <http://www.ipt.arc.nasa.gov/trent.html> and <http://amesnews.arc.nasa.gov/audio/bionanosound/bionano9.html>.

Inquiries concerning rights for the commercial use of this invention should be addressed to the Patent Counsel, Ames Research Center, (650) 604-5104. Refer to ARC-14744.



This Planar Array of Gold Nanoparticles was formed on a carbon film by the method summarized in the text.

Low-Temperature Plasma Functionalization of Carbon Nanotubes

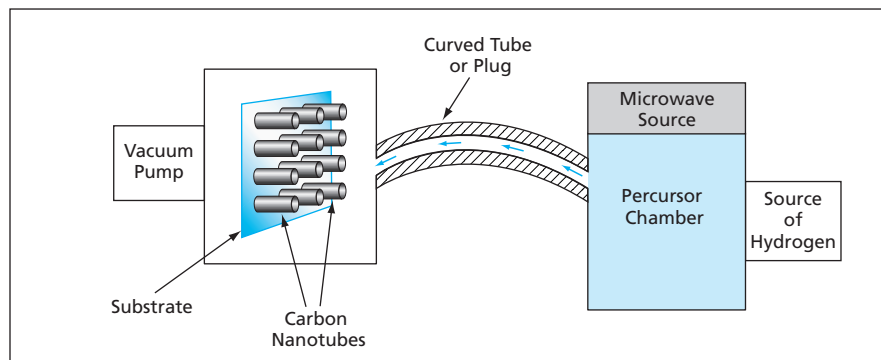
This process is dry, clean, and relatively simple.

Ames Research Center, Moffett Field, California

A low-temperature plasma process has been devised for attaching specified molecular groups to carbon nanotubes in order to impart desired chemical and/or physical properties to the nanotubes for specific applications. Unlike carbon-nanotube-functionalization processes reported heretofore, this process does not involve the use of wet chemicals, does not involve exposure of the nanotubes to high temperatures, and generates very little chemical residue. In addition, this process can be carried out in a relatively simple apparatus and can readily be scaled up to mass production.

The apparatus used in this process includes two vacuum chambers, denoted the target chamber and the precursor chamber. A plasma of the chemical precursor of the molecular groups to be deposited is generated in the precursor chamber. The plasma flows from the precursor chamber to the target chamber, wherein the carbon nanotubes to be functionalized are mounted on a substrate.

The process is best described by use of an example of functionalizing carbon nanotubes with hydrogen atoms. The precursor chamber is backfilled with high-purity (99.9999 percent or greater) H_2 gas, optionally mixed with an inert carrier gas (N_2 , Ne, or Ar), to a total gas pressure between 0.1 and 1 mm of Hg (between about 13 and about 130 Pa). The gas is irradiated with microwaves, thereby generating free electrons and a partially ionized gas that includes free radicals (in particular, monatomic hydrogen). Instead of a microwave source, a DC, non-microwave-radio-frequency, inductive-discharge, or electron-cyclotron-resonance source can also be used to generate the plasma. The tem-



A **Hydrogen Plasma** is generated in the precursor chamber and flows into the target chamber, where hydrogen atoms become chemically bonded to the carbon nanotubes.

perature of the free electrons is typically of the order of a few electron volts ($1 \text{ eV} = 11,604 \text{ K}$). The temperature of the partially ionized gas typically lies in the approximate range from 350 to 1,000 K.

The two chambers are connected by a curved tube or plug made of polytetrafluoroethylene or other suitable material. Typically, the tube or plug has an inner diameter of about 1 mm, an outer diameter of between 5 and 25 mm, and a length between 5 and 25 mm. The substrate holding the carbon nanotubes is positioned to face directly into the plasma flowing into the target chamber through the hole in the tube or plug.

The tube or plug is curved to eliminate a direct line of sight between the interiors of the chambers in order to prevent ultraviolet light originating in the precursor chamber from reaching the carbon nanotubes. This is necessary for the following reasons: Some ultraviolet radiation is generated in the undesired but unavoidable recombination of some of the monatomic hydrogen into H_2 molecules. This radiation is capable of breaking the C-H bonds in hydro-

genated materials, including hydrogenated carbon nanotubes. Other ultraviolet radiation generated in the precursor chamber may be capable of breaking C-C bonds in the nanotubes.

There is no need to maintain the temperature in the target chamber at any particular value in order to achieve functionalization. Experiments have shown that carbon nanotubes can be functionalized with hydrogen to the point of saturation in a process time of about 30 seconds, at or below room temperature. It is also possible to functionalize carbon nanotubes with molecular groups other than hydrogen. For example, by choosing a suitable precursor, one could attach halogen or alkali metal atoms or low-molecular weight hydrocarbons.

This work was done by Bishun Khare of SETI Institute and M. Meyyappan of Ames Research Center. For further information, please contact M. Meyyappan at (650) 604-2616 or E-mail: meyya@orbit.arc.nasa.gov.

Inquiries concerning rights for the commercial use of this invention should be addressed to the Patent Counsel, Ames Research Center, (650) 604-5104. Refer to ARC-14661-1.



Improved Cryostat for Cooling a Wide Panel

Less technician time and lower consumption of helium translate to lower cost.

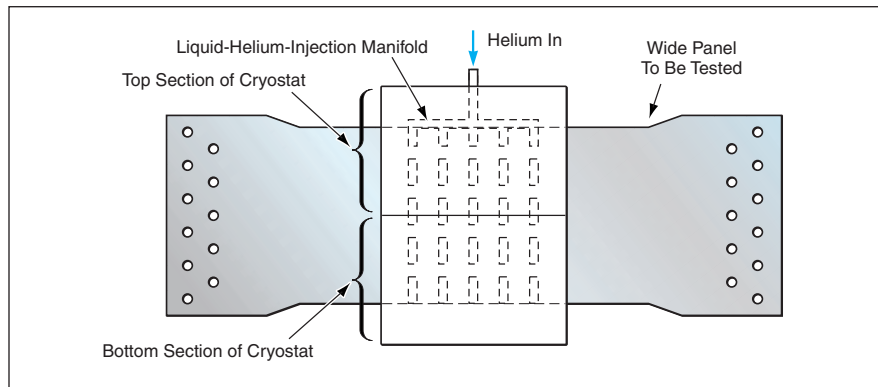
Marshall Space Flight Center, Alabama

An improved cryostat has been developed for cooling a wide panel evenly over its surface to a temperature of $-423\text{ }^{\circ}\text{F}$ ($\approx -253\text{ }^{\circ}\text{C}$) by use of liquid helium. Originally, the cryostat was to be used in measuring apparent strains in wide aluminum/lithium panels as functions of temperature in order to develop data for temperature compensation of the readings of strain gauges on a tank containing liquid hydrogen. Relative to the cryostat used previously for this purpose, the improved cryostat can be prepared for a test in less time, and it loses less helium during each test.

Each wide panel to be tested is instrumented with thermocouples in preparation for a test. The previous cryostat was made of two aluminum halves that, for each test, were sandwiched together and sealed around the instrumented wide panel to be tested. The panel was thus enclosed in a plenum. The cryostat and adjacent panel areas protruding from the cryostat were then coated with a thermally insulating foam.

During a test, liquid helium was made to flow into the plenum through a port on the bottom. The helium vaporized and expanded, filling the plenum with cold helium gas, which eventually flowed out of the plenum through a port on the top. The nature of the flow was such that a significant portion of the helium did not come into contact with the wide panel; hence, cooling was less efficient than it might otherwise have been.

After completion of each test, the foam and the cryostat were separated from the panel. The cryostat was cleaned and prepared for installation



The **Liquid-Helium-Injection Manifold** in the improved cryostat forces the helium to flow in a pattern in which it cools the panel more efficiently than in the previous cryostat.

on another instrumented wide panel for the next test. It took 28 hours to install the cryostat onto the instrumented panel, apply the foam, and perform ancillary operations in preparation for a test. The volume of liquid helium consumed during each test was 750 liters.

The improved cryostat (see figure) includes an upper section and a lower section, both of which include permanent housings made of a thermally insulating foam 2-in. ($\approx 5\text{-cm}$) thick. A liquid-helium-injection manifold is attached to the inside of the top section. The bottom section includes an outlet for helium gas. The manifold contains slots that, when the cryostat is installed on the panel, are located approximately 1 in. ($\approx 2.5\text{ cm}$) from the wide panel. The array of slots spans a substantial portion of the area of the panel. The top and bottom sections of the cryostat are sealed to the panel by use of polytetrafluoroethylene cord and

aluminum tape.

Liquid helium is fed into the manifold from the top. The helium leaves the manifold through the slots and thus impinges directly on the panel. Hence, all the helium entering the cryostat must come into contact with the panel before leaving the cryostat. After a test, the cryostat is removed from the panel and reinstalled onto another panel for the next test. Installation of the cryostat on an instrumented panel takes a negligible amount of time, in comparison with the 28 hours associated with the previous cryostat. The amount of liquid helium consumed during a test in the improved cryostat is 500 liters — 250 liters less than before.

This work was done by W. B. Clifton of Lockheed Martin Corp. for Marshall Space Flight Center. Further information is contained in a TSP (see page 1). MFS-31697

Current Pulses Momentarily Enhance Thermoelectric Cooling

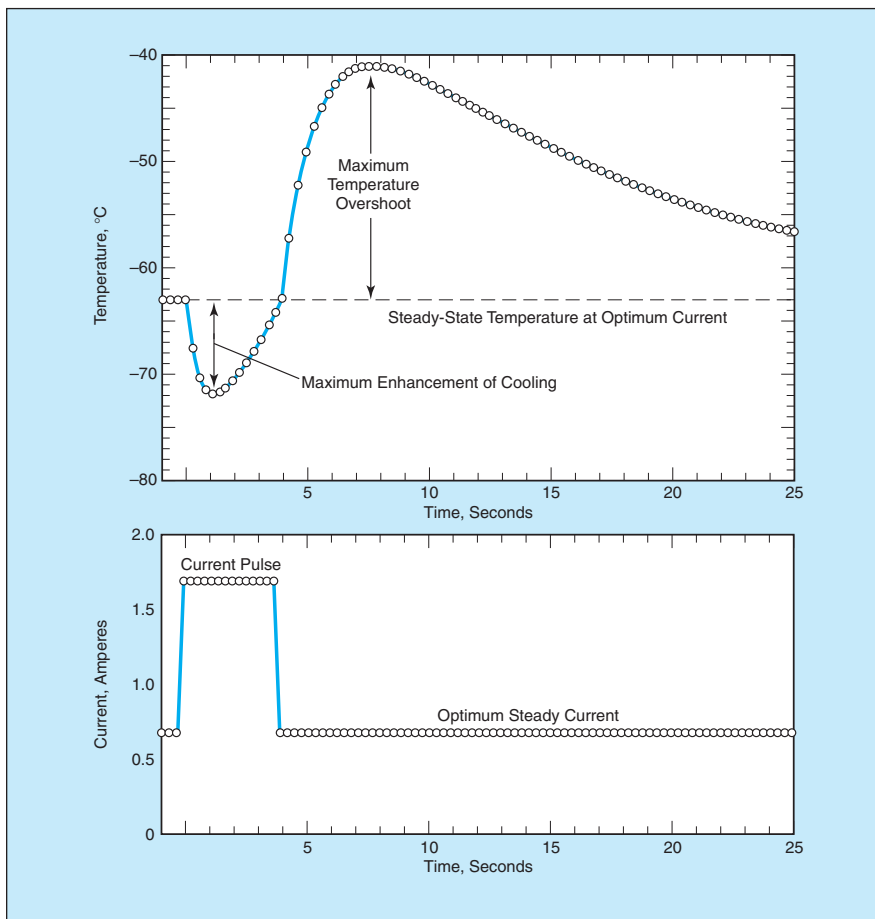
Transient cooling could be attractive for some semiconductor devices.

NASA's Jet Propulsion Laboratory, Pasadena, California

The rates of cooling afforded by thermoelectric (Peltier) devices can be increased for short times by applying pulses of electric current greater than the currents that yield maximum steady-state

cooling. It has been proposed to utilize such momentary enhancements of cooling in applications in which diode lasers and other semiconductor devices are required to operate for times of the order

of milliseconds at temperatures too low to be easily obtainable in the steady state. In a typical contemplated application, a semiconductor device would be in contact with the final (coldest) somewhat



A Pulse of Current greater than the optimum steady current was applied to a thermoelectric device, giving rise to transient enhancement of cooling followed by transient heating followed by gradual decay toward the steady state.

taller stage of a multistage thermoelectric cooler. Steady current would be applied to the stages to produce steady cooling. Pulsed current would then be applied, enhancing the cooling of the top stage momentarily.

The principles of operation are straightforward: In a thermoelectric device, the

cooling occurs only at a junction at one end of the thermoelectric legs, at a rate proportional to the applied current. However, Joule heating occurs throughout the device at a rate proportional to the current squared. Hence, in the steady state, the steady temperature difference that the device can sustain increases with current

only to the point beyond which the Joule heating dominates. If a pulse of current greater than the optimum current (the current for maximum steady cooling) is applied, then the junction becomes momentarily cooled below its lowest steady temperature until thermal conduction brings the resulting pulse of Joule heat to the junction and thereby heats the junction above its lowest steady temperature.

A theoretical and experimental study of such transient thermoelectric cooling followed by transient Joule heating in response to current pulses has been performed. The figure presents results from one of the experiments. The study established the essential parameters that characterize the pulse cooling effect, including the minimum temperature achieved, the maximum temperature overshoot, the time to reach minimum temperature, the time while cooled, and the time between pulses. It was found that at large pulse amplitude, the amount of pulse supercooling is about a fourth of the maximum steady-state temperature difference. For the particular thermoelectric device used in one set of the experiments, the practical optimum pulse amplitude was found to be about 3 times the optimum steady-state current. In a further experiment, a pulse cooler was integrated into a small commercial thermoelectric three-stage cooler and found to provide several degrees of additional cooling for a time long enough to operate a semiconductor laser in a gas sensor.

This work was done by G. Jeffrey Snyder, Jean-Pierre Fleurial, and Thierry Caillat of Caltech, and Gang Chen and Rong Gui Yang of MIT for NASA's Jet Propulsion Laboratory. Further information is contained in a TSP (see page 1). NPO-30553

Hand-Held Color Meters Based on Interference Filters

These inexpensive units measure luminous flux in several wavelength bands.

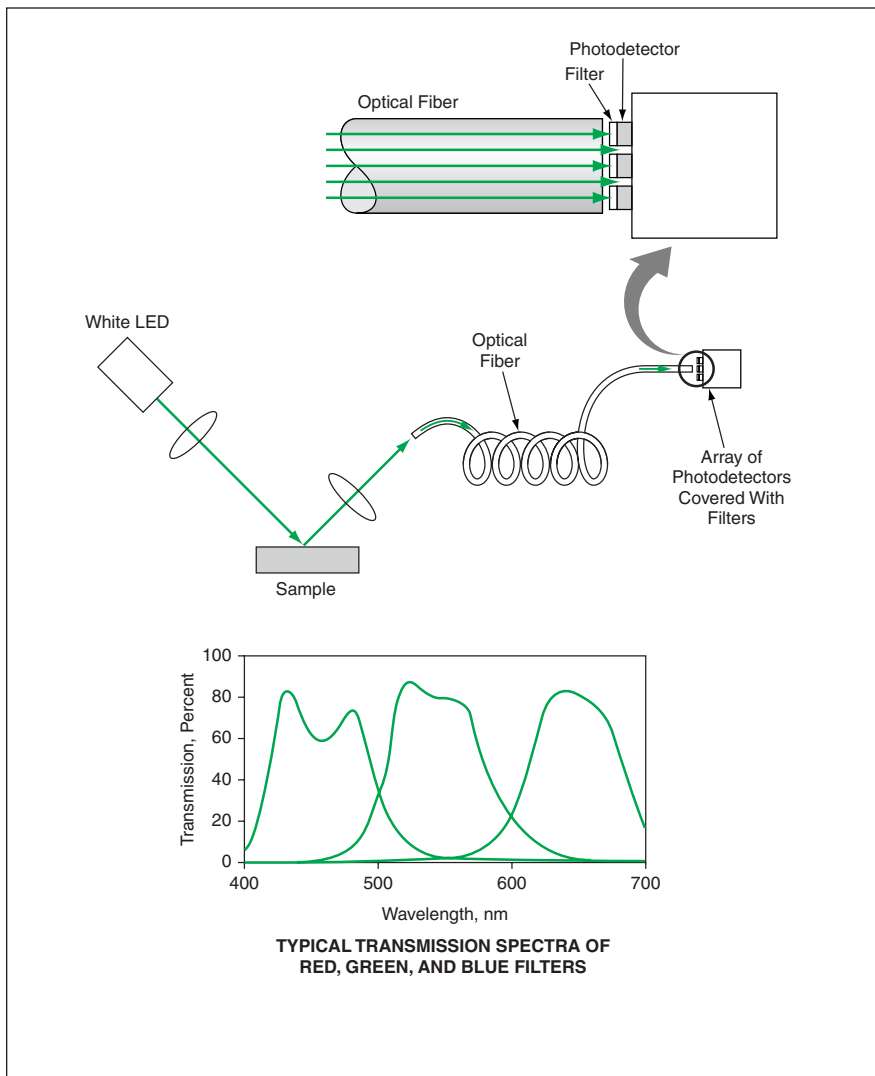
NASA's Jet Propulsion Laboratory, Pasadena, California

Small, inexpensive, hand-held optoelectronic color-measuring devices based on metal-film/dielectric-film interference filters are undergoing development. These color meters could be suitable for use in a variety of applications in which there are requirements to quantify or match colors for aesthetic purposes but there is no need for the high spectral resolution of scientific-grade spectrometers. Such applications

typically occur in the paint, printing, and cosmetic industries, for example.

The figure schematically depicts a color meter of this type being used to measure the color of a sample in terms of the spectrum of light reflected from the sample. Light from a white source (for example, a white light-emitting diode) passes through a collimating lens to the sample. Another lens collects some of the light reflected from the sample and

focuses the light onto the input end of optical fiber. Light emerging from the output end of the optical fiber illuminates an array of photodetectors covered with metal/dielectric-film interference filters like those described in "Metal/Dielectric-film Interference Color Filters" (NPO-20217), *NASA Tech Briefs*, Vol. 23, No. 2 (February 1999), page 70. Typically, these are wide-band-pass filters, as shown at the bottom of the figure.



Several Photodetectors Covered by Filters measure incident light in several wavelength bands. In this example, there are three broad wavelength bands corresponding approximately to the primary additive colors.

The photodetector array need not be of any particular design: it could be something as simple as an assembly containing several photodiodes or something as elaborate as an active-pixel sensor or other imaging device. What is essential is that each of the photodetectors or each of several groups of photodetectors is covered with a metal/dielectric-film filter of a different color. In most applications, it would be desirable to have at least three different filters, each for a spectral band that contains one of the three primary additive red, green, and blue colors. In some applications, it may be necessary to have more than three different color filters in order to characterize subtle differences in color (or in the sensation of color) that cannot be characterized with sufficient precision by use of the primary colors alone.

This work was done by Yu Wang of Caltech for NASA's Jet Propulsion Laboratory. Further information is contained in a TSP (see page 1).

In accordance with Public Law 96-517, the contractor has elected to retain title to this invention. Inquiries concerning rights for its commercial use should be addressed to:

*Innovative Technology Assets Management
JPL*

Mail Stop 202-233

4800 Oak Grove Drive

Pasadena, CA 91109-8099

(818) 354-2240

E-mail: iaoffice@jpl.nasa.gov

Refer to NPO-30858, volume and number of this NASA Tech Briefs issue, and the page number.

Calculating Mass Diffusion in High-Pressure Binary Fluids

This model could contribute to understanding of high-pressure combustion.

NASA's Jet Propulsion Laboratory, Pasadena, California

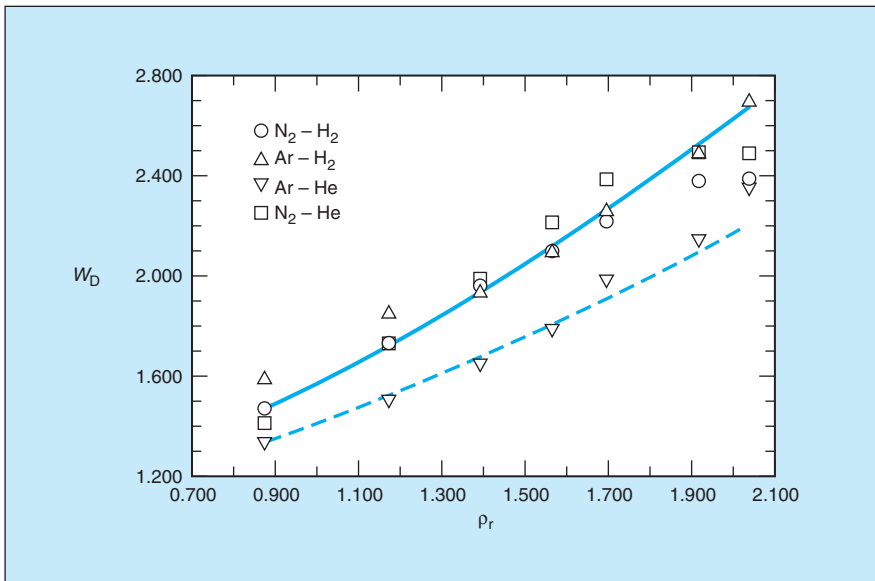
A comprehensive mathematical model of mass diffusion has been developed for binary fluids at high pressures, including critical and supercritical pressures. Heretofore, diverse expressions, valid for limited parameter ranges, have been used to correlate high-pressure binary mass-diffusion-coefficient data. This model will likely be especially useful in the computational simulation and analysis of combustion phenomena in diesel engines, gas turbines, and liquid rocket engines, wherein mass diffusion at high pressure plays a major role.

The model recasts the kinetic theory (i.e. low-pressure) expressions into forms consistent with the principle of corresponding states. Also presented are corresponding states forms for the Stokes-Einstein hydrodynamic model for diffusion in liquids, which are used for purposes of comparison. By ansatz, the model includes an expression that reflects departures from the kinetic-theory diffusion-coefficient relationship by means of a division factor that is partly a function of the reduced species density, becomes unity in the limit of low-

pressure gases, and includes parameters to be determined empirically for higher pressures. The final model equation is

$$D_{ij}^0 = (D_{ij})_{KT} / w_{D,j}$$

where D_{ij}^0 is the high-pressure infinite dilution diffusivity of species i in j , $(D_{ij})_{KT}$ is the binary diffusivity calculated according to kinetic theory, and $w_{D,j} = 1 + \delta_{D,j}$ is the division factor. As the reduced density of species j approaches zero, so does $\delta_{D,j}$. Empirical parameters have been determined



The Division Factor (w_D) was calculated as a function of reduced density (ρ_r) for several binary fluid mixtures. The curves were calculated by use of $\delta_D = c\rho_r^{3/2}$, where $c = 0.42$ and $c = 0.58$.

and the model evaluated by means of correlations with experimental data from the literature (see figure). Typical uncertainties in the correlations have been estimated to lie between 10 and 15 percent and to reach a maximum of about 30 percent at high density.

Simulations of heptane drops in nitrogen under zero gravity and at high pressure were performed using the model in order to investigate the sensitivities of predicted drop diameters to uncertainties in diffusivity values. The results of the simulations showed that the root-mean-square deviations of relative drop diameters were approximately one-fourth of the corresponding imposed relative changes in diffusivities.

This work was done by Josette Bellan and Kenneth Harstad of Caltech for NASA's Jet Propulsion Laboratory. Further information is contained in a TSP (see page 1). NPO-30409

Fresnel Lenses for Wide-Aperture Optical Receivers

These would be relatively inexpensive, lightweight alternatives to conventional telescope lenses.

NASA's Jet Propulsion Laboratory, Pasadena, California

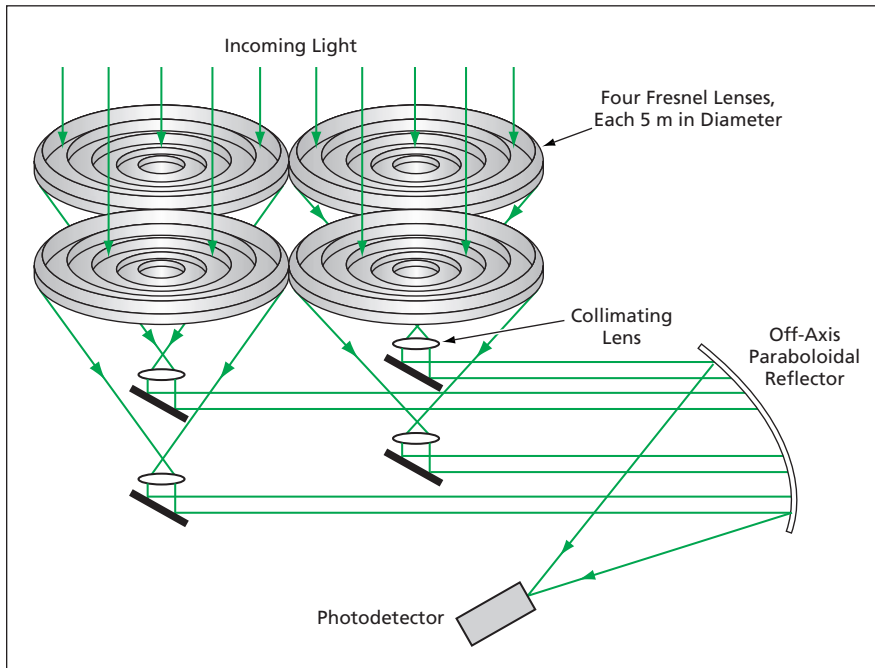
Wide-aperture receivers for free-space optical communication systems would utilize Fresnel lenses instead of conventional telescope lenses, according to a proposal. Fresnel lenses weigh and cost much less than conventional

lenses having equal aperture widths. Plastic Fresnel lenses are commercially available in diameters up to 5 m — large enough to satisfy requirements for aperture widths of the order of meters for collecting sufficient light in typ-

ical long-distance free-space optical communication systems.

Fresnel lenses are not yet suitable for high-quality diffraction-limited imaging, especially in polychromatic light. However, optical communication systems utilize monochromatic light, and there is no requirement for high-quality imaging; instead, the basic requirement for an optical receiver is to collect the incoming monochromatic light over a wide aperture and concentrate the light onto a photodetector.

Because of lens aberrations and diffraction, the light passing through any lens is focused to a blur circle rather than to a point. Calculations for some representative cases of wide-aperture non-diffraction-limited Fresnel lenses have shown that it should be possible to attain blur-circle diameters of less than 2 mm. Preferably, the blur-circle diameter should match the width of the photodetector. For most high-bandwidth communication applications, the required photodetector diameters would be about 1 mm. In a less-preferable case in which the blur circle was wider than a single photodetector, it would be possible to occupy the blur circle with an array of photodetectors.



Incoming Light Would Be Collected by four Fresnel lenses, then the light would be collimated and concentrated onto a single photodetector.

As an alternative to using a single large Fresnel lens, one could use an array of somewhat smaller lenses to synthesize the equivalent aperture area. Such a configuration might be preferable in a case in which a single Fresnel lens of the requisite large size would be impractical to manufacture, and the blur circle could not be made small enough. For example one could construct a square array of four 5-m-diameter Fresnel lenses to obtain the same light-collecting area as that of a single 10-m-diameter lens. In that case (see fig-

ure), the light collected by each Fresnel lens could be collimated, the collimated beams from the four Fresnel lenses could be reflected onto a common off-axis paraboloidal reflector, and the paraboloidal reflector would focus the four beams onto a single photodetector. Alternatively, detected signal from each detector behind each lens would be digitized before summing the signals.

This work was done by Hamid Hemmati of Caltech for NASA's Jet Propulsion Laboratory. Further information is contained in a TSP (see page 1).

In accordance with Public Law 96-517, the contractor has elected to retain title to this invention. Inquiries concerning rights for its commercial use should be addressed to:

*Innovative Technology Assets Management
JPL*

Mail Stop 202-233

4800 Oak Grove Drive

Pasadena, CA 91109-8099

(818) 354-2240

E-mail: iaoffice@jpl.nasa.gov

Refer to NPO-40436, volume and number of this NASA Tech Briefs issue, and the page number.



Increasing Accuracy in Computed Inviscid Boundary Conditions

Accuracy is increased through use of higher-order time derivatives.

John H. Glenn Research Center, Cleveland, Ohio

A technique has been devised to increase the accuracy of computational simulations of flows of inviscid fluids by increasing the accuracy with which surface boundary conditions are represented. This technique is expected to be especially beneficial for computational aeroacoustics, wherein it enables proper accounting, not only for acoustic waves, but also for vorticity and entropy waves, at surfaces.

Heretofore, inviscid nonlinear surface boundary conditions have been limited to third-order accuracy in time for stationary surfaces and to first-order accuracy in time for moving surfaces. For steady-state calculations, it may be possible to achieve higher accuracy in space, but high accuracy in time is needed for efficient simulation of multiscale unsteady flow phenomena. The present technique is the first surface treatment that provides the needed high accuracy through proper accounting of higher-order time derivatives.

The present technique is founded on a method known in art as the Hermitian modified solution approximation (MESA)

scheme. This is because high time accuracy at a surface depends upon, among other things, correction of the spatial cross-derivatives of flow variables, and many of these cross-derivatives are included explicitly on the computational grid in the MESA scheme. (Alternatively, a related method other than the MESA scheme could be used, as long as the method involves consistent application of the effects of the cross-derivatives.)

While the mathematical derivation of the present technique is too lengthy and complex to fit within the space available for this article, the technique itself can be characterized in relatively simple terms: The technique involves correction of surface-normal spatial pressure derivatives at a boundary surface to satisfy the governing equations and the boundary conditions and thereby achieve arbitrarily high orders of time accuracy in special cases. The boundary conditions can now include a potentially infinite number of time derivatives of surface-normal velocity (con-

sistent with no flow through the boundary) up to arbitrarily high order. The corrections for the first-order spatial derivatives of pressure are calculated by use of the first-order time derivative velocity. The corrected first-order spatial derivatives are used to calculate the second-order time derivatives of velocity, which, in turn, are used to calculate the corrections for the second-order pressure derivatives. The process as described is repeated, progressing through increasing orders of derivatives, until the desired accuracy is attained.

This work was done by Roger Dyson of Glenn Research Center and Ray Hixon of the Institute for Computational Mechanics in Propulsion. Further information is contained in a TSP (see page 1).

Inquiries concerning rights for the commercial use of this invention should be addressed to NASA Glenn Research Center, Commercial Technology Office, Attn: Steve Fedor, Mail Stop 4-8, 21000 Brookpark Road, Cleveland, Ohio 44135. Refer to LEW-17500-1.

Higher-Order Finite Elements for Computing Thermal Radiation

Computationally efficient methods yield close approximations of exact solutions.

Langley Research Center, Hampton, Virginia

Two variants of the finite-element method have been developed for use in computational simulations of radiative transfers of heat among diffuse gray surfaces. Both variants involve the use of higher-order finite elements, across which temperatures and radiative quantities are assumed to vary according to certain approximations. In this and other applications, higher-order finite elements are used to increase (relative to classical finite elements, which are assumed to be isothermal) the accuracies of final numerical results without having to refine computational meshes excessively and thereby incur excessive computation times.

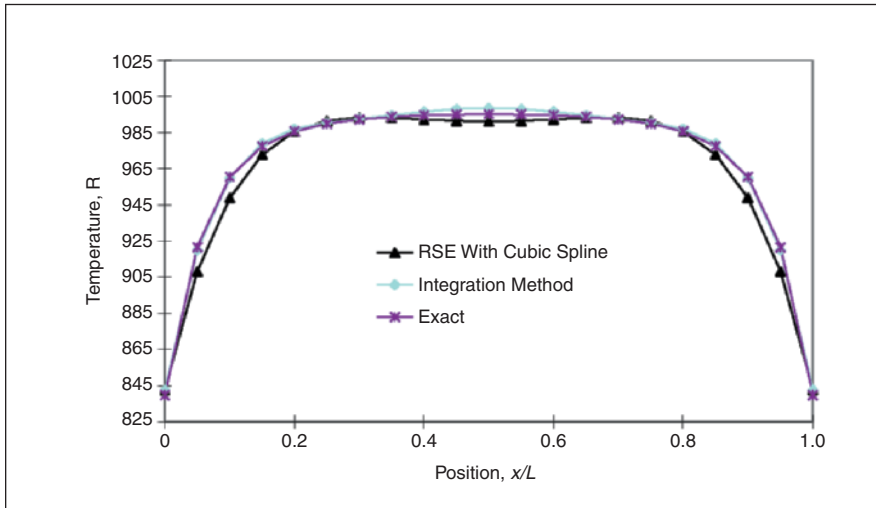
One of the variants is termed the radiation sub-element (RSE) method, which,

itself, is subject to a number of variations. This is the simplest and most straightforward approach to representation of spatially variable surface radiation. Any computer code that, heretofore, could model surface-to-surface radiation can incorporate the RSE method without major modifications.

In the basic form of the RSE method, each finite element selected for use in computing radiative heat transfer is considered to be a parent element and is divided into sub-elements for the purpose of solving the surface-to-surface radiation-exchange problem. The sub-elements are then treated as classical finite elements; that is, they are assumed to be isothermal, and their view factors and absorbed heat fluxes are calculated accordingly. The

heat fluxes absorbed by the sub-elements are then transferred back to the parent element to obtain a radiative heat flux that varies spatially across the parent element. Variants of the RSE method involve the use of polynomials to interpolate and/or extrapolate to approximate spatial variations of physical quantities.

The other variant of the finite-element method is termed the integration method (IM). Unlike in the RSE methods, the parent finite elements are not subdivided into smaller elements, and neither isothermality nor other unrealistic physical conditions are assumed. Instead, the equations of radiative heat transfer are integrated numerically over the parent finite elements by use of a computationally efficient Gaussian inte-



Temperature Versus Position along a plate was computed in a test case exactly and by two variants of the finite-element method.

gration scheme. In this scheme, the radiant heat transfer is computed at discrete points on each surface in the radiation exchange. These points corresponding to the Gauss points are used in evaluating the element matrices.

The IM is implemented in the following iterative procedure:

1. Initialize unknowns (temperatures and radiative heat fluxes).
2. Calculate differential form factors between Gauss points on all elements.
3. Calculate radiative heat fluxes at Gauss points on all elements.
4. Integrate radiative heat fluxes to obtain a radiative-heating load vector.
5. Solve for and update temperatures.
6. Examine the results for convergence. If results have not converged to within acceptably narrow margins, return to step 3.

In a test problem, an upper plate of length L was assumed to be maintained isothermal at a temperature of 1,000 R

(≈ 556 K) and a lower plate of the same length was assumed to be placed at the same horizontal position at a distance $0.1L$ below the upper plate and allowed to come to thermal equilibrium. The figure depicts the temperature of the lower plate versus position along the plate as calculated by the RSE method with cubic-spline interpolation and by the IM with 16 Gauss points. Also shown is the exact solution. Both methods show reasonably good agreement with the exact solution, with the integration method nearly indistinguishable from the exact solution over most of the plate. In general, the integration method proved to be more accurate with respect to spatial variation; however, it was also more costly (longer run times). Both methods captured temporal variations equally well. These results indicate that the RSE method is preferred for efficient analyses in which temperature variations are mainly temporal, while the integration method is reserved for analyses requiring very accurate resolution of spatial gradients.

This work was done by Dana C. Gould of Langley Research Center. For further information, access the Technical Support Package (TSP) free on-line at www.techbriefs.com/tsp under the Information Sciences category.
LAR-16101



Radar for Monitoring Hurricanes From Geostationary Orbit

A document describes a scanning Doppler radar system to be placed in a geostationary orbit for monitoring the three-dimensional structures of hurricanes, cyclones, and severe storms in general. The system would operate at a frequency of 35 GHz. It would include a large deployable spherical antenna reflector, instead of conventional paraboloidal reflectors, that would allow the reflector to remain stationary while moving the antenna feed(s), and thus, create a set of scanning antenna beams without degradation of performance. The radar would have separate transmitting and receiving antenna feeds moving in spiral scans over an angular excursion of 4° from the boresight axis to providing one radar image per hour of a circular surface area of 5,300-km diameter. The system would utilize a real-time pulse-compression technique to obtain 300-m vertical resolution without sacrificing detection sensitivity and without need for a high-peak

power transmitter. An onboard data-processing subsystem would generate three-dimensional rainfall reflectivity and Doppler observations with 13-km horizontal resolution and line-of-sight Doppler velocity at a precision of 0.3 m/s.

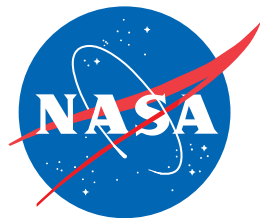
This work was done by Eastwood Im, Stephen Durden, John Huang, Michael Lou, Eric Smith, and Yahya Rahmat-Samii of Caltech for NASA's Jet Propulsion Laboratory. Further information is contained in a TSP (see page 1). NPO-40423

Time-Transfer System for Two Orbiting Spacecraft

A report describes the time-transfer system of the Gravity Recovery and Climate Experiment (GRACE), in which information on the distribution of Earth mass is extracted from position and time measurements for two spacecraft about 200 km apart in a circular, nearly polar orbit. Each spacecraft carries a Global Positioning System (GPS) receiver, a K/Ka-band ranging

(KBR) instrument, and an ultra-stable oscillator (USO) that serves as a clock for the GPS and KBR units. The long-term errors of the USOs are cancelled by use of a technique, called dual-one-way phase measurements, in which the phases of the KBR signals from spacecraft A as measured at spacecraft B are added to the phases of the KBR signals from spacecraft B as measured at spacecraft A. GPS data are used to synchronize time between the USOs to within ≈150 ps as needed to enable the dual-one-way phase measurements: For each spacecraft, the GPS data are used to solve for orbital positions, and the difference between the onboard clocks and a ground clock every 5 minutes. The relative clock rate between the spacecraft is then determined from the difference between the two solutions.

This work was done by William Bertiger, Seen-Chong Wu, Gerhard Kruizinga, Charles Dunn, and Larry Romans of Caltech for NASA's Jet Propulsion Laboratory. Further information is contained in a TSP (see page 1). NPO-40344



National Aeronautics and
Space Administration